Funded by the Horizon 2020 Framework Programme of the European Union
Grant Agreement No. 871158

AHEAD 2020 Scientific/Technical Report - WP 9.8

Understanding the interaction between soft protons and X-ray mirrors

Final report

Reference Period: 02/03/2020 – 01/09/2022

V.Fioretti[1], T. Mineo[2], R. Amato[2], S. Lotti[3], C. Macculi[3], S. Molendi[4], F. Gastaldello[4], G. Lanzuisi[1], M. Cappi[1], M. Dadina[1], S. Ettori[1]

[1]INAF OAS Bologna, [2]INAF IASF Palermo, [3]INAF IAPS Roma, [4]INAF IASF Milano

Project acronym:
AHEAD2020

Version: 1.2
Date: 3/10/2022

Project Title:
Integrated Activities for the High Energy Astrophysics Domain

Grant Agreement No: **871158**
This deliverable is part of a project that has received funding from the European Union's Horizon 2020 research and innovation programme

Start date of the project:
2020-03-02

Version	Revision Date	Review/Approval
1.0	1/09/2022	Creation date
1.1	3/10/2022	Internal review
1.2	14/10/2022	Included comments by WP leaders

Distribution List	Date	Version
AHEAD2020 WP 9	5/10/2022	1.1
AHEAD2020 WP 9	14/10/2022	1.2

0. Explanation of the work carried out within the WP 5
0.1 Activity breakdown 6
1. XMM-Newton proton response matrix design (Task 1) 8
1.1 EPIC soft proton spectra extraction (Task 1.1) 8
1.2 Geant4 XMM soft proton scattering (Task 1.2) 10
1.3 Ray-tracing XMM soft proton scattering (Task 1.3) 11
1.4 Geant4 proton attenuation simulation (Task 1.4) 13
1.4.1 MOS focal plane assembly 13
1.4.2 PN focal plane assembly 18
2. ATHENA proton response matrix design (Task 2) 20
2.1 Geant4 ATHENA soft proton scattering (Task 2.1) 20
2.2 Ray-tracing ATHENA soft proton scattering (Task 2.2) 21
2.3 Geant4 X-IFU proton scattering simulation (Task 2.3) 23
2.4 Geant4 WFI proton scattering simulation (Task 2.4) 24
3. Data formatting, verification and validation (Task 3) 26
3.1 Data input formatting (Task 3.1) 26
3.2 XMM-Newton and ATHENA proton response matrix (Task 3.2) 26
3.3 Verification of the XMM-Newton and ATHENA response files (Task 3.3) 30
3.4 Validation of the XMM-Newton proton response files (Task 3.4) 32
3.4.1 Validation with single observations 32
3.4.2 Validation with orbit averaged spectra 35
3.4.3 Summary of the validation activity 36
References 36
Deliverables 39
Dissemination & communication activities 40
Deviations and non-compliances 41

0. Explanation of the work carried out within the WP

Low energy (< 300 keV) protons entering the field of view of the XMM-Newton telescope and scattering with the mirror surface are observed in the form of a sudden increase in the background level. Such flaring events, affecting about 30-40% of the XMM-Newton observing time, can hardly be disentangled from true X-ray events and cannot be rejected on board. All future high throughput gracing incidence X-ray telescopes operating outside the radiation belts (e.g. ATHENA) are potentially affected by soft proton induced contamination that must be foreseen and limited since the design phase. On the other side, a clear description of the interaction model would link the observed soft proton spectra by XMM-Newton to the ones hitting the telescope pupil, mapping the low energy particle environment along its orbit.

Thanks to the latest validation studies on the physics models describing the reflection process of protons at grazing angles, we build a proton response matrix for the XMM-Newton and ATHENA missions, describing the effective area and energy redistribution of protons entering the mirror aperture. The simulation pipeline comprises two independent simulation frameworks for the X-ray optics reflectivity, based on ray-tracing and Geant4, and a Geant4 simulation for the proton transmission efficiency caused by the combination of optical filters, on-chip electrodes and the detection depletion regions, requiring a detailed mass model of the focal plane assemblies.

The response matrix for protons will allow a better understanding of the proton radiation environment, with the aim of modeling the in-flight non X-ray background of current and future X-ray focusing telescopes. The XMM-Newton matrix will be used to analyze the mean energy spectra of the background flares, converting the mission into a “proton telescope”, while characterizing its particle background. The matrices for the ATHENA telescope will allow for a fast evaluation of the soft proton induced background for any input population, driving the design of shielding solutions.

The response matrix is formatted according to the NASA OGIP (Office of Guest Investigators Program) calibration database (caldb) format, and it consists of an RMF and ARF file in FITS (Flexible Image Transport System) format. X-ray data analysis tools available to the X-ray astronomy community such as *Xspec* and *SPEX* can be used to simulate or analyse the soft proton-induced background spectra.

0.1 Activity breakdown

The following table shows the breakdown of the present WP, with the activity structured in three subWPs, two dedicated to the production of the proton response matrix for the XMM-Newton and ATHENA use cases, and the last dedicated to data formatting, verification and validation.

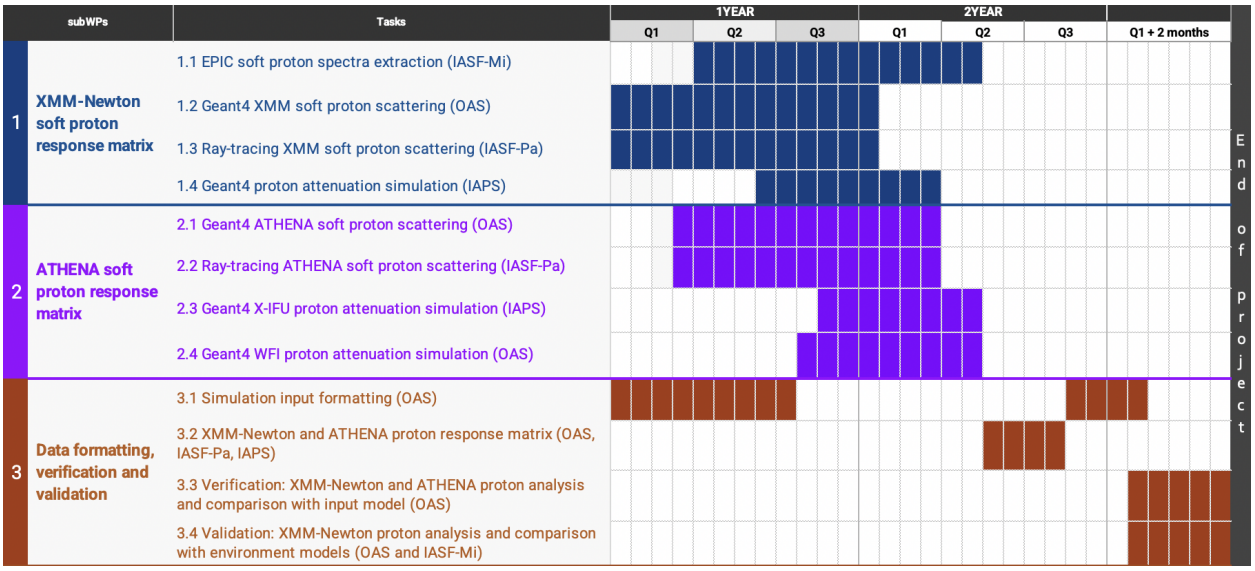

Table 1: WP breakdown.

Participants and tasks:

- INAF/OAS:
  - V. Fioretti, G. Lanzuisi, M. Dadina, M. Cappi, S. Ettori
  - Tasks:
    - Management (V. Fioretti)
    - 1.2 (V. Fioretti)
    - 2.1 (V. Fioretti)
    - 2.4 (V. Fioretti)
    - 3.1 (V. Fioretti, G. Lanzuisi)
    - 3.2 (V. Fioretti, G. Lanzuisi)
    - 3.3 (M. Dadina, M. Cappi, S. Ettori)
    - 3.4 (M. Dadina, M. Cappi, S. Ettori)

- INAF/IASF-Mi:
  - S. Molendi, F. Gastaldello
  - Tasks:
    - 1.1 (S. Molendi, F. Gastaldello)
    - 3.2 (S. Molendi, F. Gastaldello)
    - 3.4 (S. Molendi, F. Gastaldello)

- INAF/IASF-Pa:
  - T. Mineo, R. Amato
  - Tasks:
    - 1.3 (T. Mineo, R. Amato)
    - 1.4 (T. Mineo, R. Amato)
    - 2.2 (T. Mineo, R. Amato)

        - 3.2 (T. Mineo, R. Amato)

- INAF/IAPS:
    - S. Lotti, C. Macculi
    - Tasks:
        - 1.4 (S. Lotti, C. Macculi)
        - 2.3 (S. Lotti, C. Macculi)
        - 3.2 (S. Lotti, C. Macculi)

1. XMM-Newton proton response matrix design (Task 1)

The ESA XMM-Newton X-ray mission was launched in December 1999. In more than 20 years, and counting, of operations has provided a unique observation window to the X-ray Universe at energies below 10 – 15 keV. Orbiting in high eccentricity elliptical orbit, with an apogee > 105 km, XMM-Newton carries three Wolter type-I mirrors to focus X-rays by means of grazing angle reflection with European Photon Imaging Cameras (EPIC) placed at each focal plane.

The XMM-Newton EPIC instrument is the telescope X-ray imager and spectrometer, covering the 0.2 -15 keV energy range. It consists of three cameras: two MOS [1] and one PN CCD [2]. In addition to the focal plane instrumentation, two of the three telescopes are equipped with Reflection Grating Spectrometers (RGS [3]). About 50% of the proton flux is expected for the XMM-Newton EPIC/MOS [4] which is partially shaded by the RGS.

Each X-ray mirror module consists of 58 Wolter type-I coaxial and co-focal Gold-coated Nichel shells [5] composed by a paraboloid and hyperboloid section, with a thickness ranging from 0.47 mm at the inner shell, with a diameter of about 30 cm, to 1.07 mm at the outer 70 cm diameter. The coating thickness is 0.2 μm and the focal length is 7.5 m. An X-ray baffle is placed at the entrance for stray-light suppression in the field of view of the instruments. Its inclusion is mandatory in the mirror simulation because it also reduces the incoming proton flux. The baffle is made of Invar, a Nickel-Iron alloy commonly used for space applications because of its low coefficient of thermal expansion, and it consists of two planes of 59 circular strips and 16 radial spokes at about 10 cm from the mirror entrance.

During observation, the XMM-Newton filter wheel can set the optical blocking filters as:

- thin filter, with 0.16 μm of poly-imide and 0.04 μm of aluminum;
- medium filter, with 0.16 μm of poly-imide and 0.08 μm of aluminum;
- thick filter, with 0.33 μm of polypropylene, and 0.11 μm of aluminum, and 0.045 μm of tin.

Protons lose some of their energy crossing the optical filters, and each of their configuration is associated to a different set of RMF and ARF files.

1.1 EPIC soft proton spectra extraction (Task 1.1)

The EXTraS (Exploring the X-ray Transient and variable Sky) project [6] funded by the FP7 European program, provided an unbiased database of XMM-Newton EPIC blank sky observations collected from 2000 to 2012. This unprecedented collection of data was used in the ESA AREMBES[1] project to characterize both the unfocused and focused observed particle background. Soft proton flares are extremely unpredictable in duration, lasting from 100 s to hours, and intensity. In the intense flares the unfocused background can be assumed negligible and both PN and MOS observations can be analysed using the proton response matrix. If instead we want to extract a representative count rate from the 12 year data-set to compare the best-fit model with the predicted proton environment, the observations must be cleaned not only of source contamination, CXB and instrument noise, but also the level of the unfocused particle background must be kept under control. Since only the MOS detector provides an out-of-FoV region to

[1] https://space-env.esa.int/athena-radiation-environment-models-and-x-ray-background-effects-simulators-arembes/

measure the unfocused background component and because of the loss of the MOS1 CCD, only EPIC MOS2 observations were used for this study.

The focused background count rate was extracted with the following conditions:

- only single and double events and standard flags to avoid bright columns and pixels;
- $7 < E < 12$ keV to avoid CXB contamination;
- exclusion of the 9.4-10 and 11-12 energy bands to eliminate the Gold fluorescence line;
- only exposures in the Full Window mode to obtain a uniform data-set.

The product of this analysis was a FITS file containing for each 500 sec time bin the count rate of both the in-FoV and out-of-FoV observations, for a total of 106.42 Ms of exposure [7]. The in-FoV minus out-of-FoV count rate cumulative distribution function (CDF) is normalized here in units of counts cm^{-2} s^{-1} keV^{-1}, using the area coverage for the in-FoV observations of 31.2 cm^2 and the selected energy ranges in the data filtering process. The CDF is shown in Fig. 1, from which we can compute the fraction of time spent by the XMM-Newton telescope below a given count rate. The maximum focused background count rate expected in 90% of the observing time is 0.0164 counts cm^{-2} s^{-1} keV^{-1}. In the verification and validation process of Sect. 3 we test the proton response matrix with two different input models of the soft proton environment linked to the magnetosheath regime of the Earth's magnetosphere and the interplanetary solar wind. Since these models refer to the maximum flux expected in 90% of observation time, the simulated background at MOS is compared to the observed CDF 90% count rate, to test the accuracy of the response files but also explore the origin of XMM soft proton flares.

Spectral analysis of in-flight soft proton flares deconvolved with the proton response matrix is also an important validation and study tool. We exploited 13 spectra extracted in [7] from the 12 years data-set for each optical filter combination, on the basis of the discrepancy between the in-FoV and out-of-FoV regions and the intensity of the in-FoV region. We selected the spectrum with a ratio between the in-FoV and out-of-FoV counts between 10 and 20, where we can neglect the unfocused background contamination. The spectrum was then normalized for the CDF 90% rate to obtain a representative intensity. We assume that any dependence of the spectral distribution on the intensity is much lower than the general uncertanties of the present study. The normalised spectrum, obtained from about 200 ks of data, is plotted in Fig. 2.

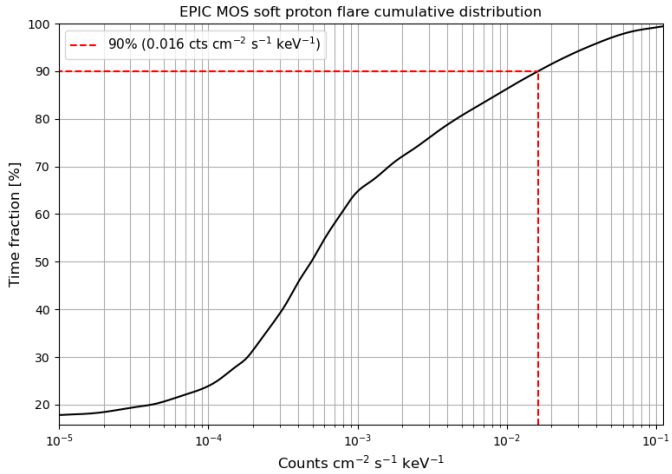

Figure 1: CDF of the EPIC MOS2 focused background count rate. The dashed lines refer to the maximum rate expected in 90% of exposure time.

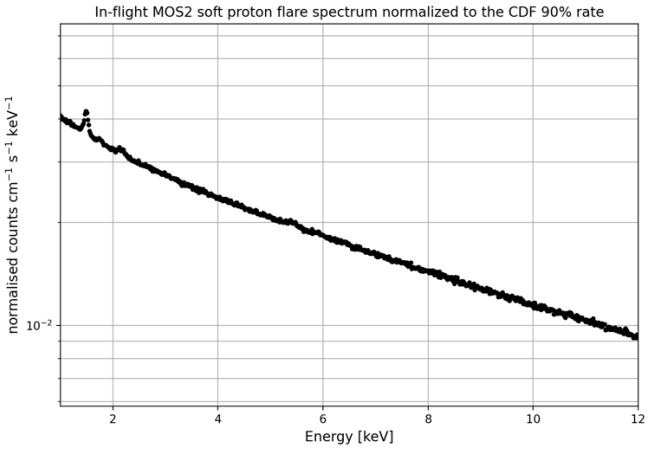

Figure 2: MOS2 X-ray spectrum (medium filter) of high state soft proton flares covering about 200ks of observation, normalised to the CDF 90% count rate.

1.2 Geant4 XMM soft proton scattering (Task 1.2)

The Geant4 toolkit [8, 9] is an open-source particle transport code for Monte Carlo simulations. It allows building 3D models of the instruments, tracking the particle history and storing the results of its interaction. The Geant4-based BoGEMMS framework [10] was used for the Geant4 simulations obtained throughout the work.

The Geant4 mass model of a single XMM-Newton mirror module is shown in Fig. 3 (left), with in grey the X-ray baffle, dark red the Nickel shells and yellow the Gold coating visible in the inner regions. The Wolter-I design is approximated with four cone trunks, intersecting the paraboloid and hyperboloid actual geometry. Fig. 3 (right) shows the simulated spatial distribution of the protons at the mirror exit, for an input mono-energetic beam.

The ability to reproduce the proton scattering interaction with the mirror surface is a key ingredient in the simulation of soft proton induced background. Measurements of proton scattering at grazing angles ($< 1 - 2$ degrees) on the surface of samples of the ATHENA Silicon Pore Optics and eROSITA X-ray mirror [11] and the comparison with Geant4 simulations [12], have defined the driving physics model for the reflection of protons at grazing incident angles. The new detailed validation of Geant4 physics scattering models together with a comprehensive estimate of the systematic uncertainties introduced by the experiments, proved the Coulomb scattering to reproduce experimental observations with sufficient accuracy.

Since the AREMBES and EXACRAD [13] projects provided an extensive validation of the Geant4 10.4 release, we used the same Geant4 version to produce the proton response files, selecting the Single Scattering reference physics list as the electromagnetic physics models of choice, since the Coulomb scattering modelled by the Single Scattering physics list was able to reproduce the eRosita and ATHENA SPO scattering measurement within 1σ [14].

The angular, spatial and intensity distribution of the protons at a given height from the XMM-Newton optical filter were compared to ray-tracing simulations (Sect. 1.3). Since the only impacting difference is in the proton flux intensity because of the different models implementing the proton grazing scattering, we chose the Geant4 mirror simulation as the driver for the proton response matrix production.

A set of mono-energetic runs at each input energy is produced. The proton position, energy, and angular momenta are recorded as a list of events at two heights: 754 mm, the focal plane baffle entrance, and 111 mm, at the optical filter. The comparison of the final count rate between the two cases allows estimating the impact of secondary scattering at the baffle in the focused background flux.

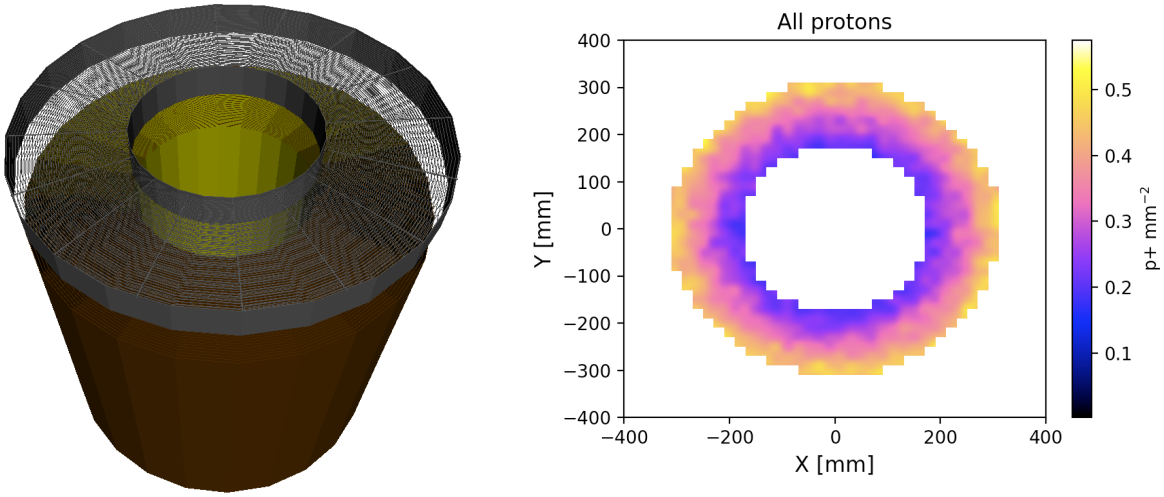

Figure 3: (left) Geant4 mass model of the XMM-Newton mirror module including the X-ray baffle placed at the telescope pupil. (right) Geant4 simulation of the proton spatial distribution at the mirror exit.

1.3 Ray-tracing XMM soft proton scattering (Task 1.3)

The ray-tracing code is a stand-alone software that includes the XMM-Newton optics geometry, the optics baffle and the forward proton shield in front of the detectors. It is able to handle either photon and protons. It follows the particle from the pupil through its interactions with the mirror shells down to the focal plane. At each interaction, it uses a Monte Carlo method to assign the particle angular and energy distribution according to a defined probability model. The photon reflectivity is modelled according to tabulated values [15, 16] and the mirror micro-roughness is taken into account modifying the output specular direction with a Gaussian. The optics geometry has been verified comparing the ray-tracing values of the X-ray on-axis effective area and vignetting at 1.5 keV and 6.4 keV with the nominal ones[2]. Discrepancies between the two sets of curves are always lower than 5%. Two proton reflection models are implemented in the XMM-Newton mirror simulation code:

- the Remizovich model in elastic approximation that assumes a reflection efficiency of 100% and no energy degradation. The output angular distribution is drawn from the Remizovich formulas [17].
- a modified version of the Remizovich model in non-elastic approximation, based on laboratory measurements on eROSITA mirror samples that include the energy lost in the interactions [18]. In

[2] Effective area curve from http://xmm.esac.esa.int/external/xmm_user_support/documentation/technical/Mirrors/index.shtml
Vignetting curves from https://xmm-tools.cosmos.esa.int/external/xmm_user_support/documentation/uhb/effareaoffaxis.html

this model the dimensionless parameter σ of the Remizovich solution, that summarizes the physics of the proton interaction with matter, is directly determined by fitting experimental data.

The elastic solution was used in a first version of the XMM-Newton proton response matrix [19] that tested the feasibility of the method. Both implementations were tested in the XMM ray-tracing simulation, but since the final proton distribution is only slightly affected, we chose to use the elastic solution since it considerably decreases the simulation time.

If the same elastic Remizovich model is implemented in the ray-tracing and Geant4 simulation of proton scattering at the XMM mirror, we find a discrepancy of about 15% in scattering efficiency likely caused by the geometrical approximation of the Wolter-I in the Geant4 simulation. If instead the Single Scattering is used in the Geant4 simulation, the scattering efficiency, i.e. the number of protons reaching the focal plane, decreases of a factor 2. Using an input energy of 50 keV at the mirror entrance, we computed and compared the angular and radial distribution of the protons at the top of the optical filters obtained with the Remizovich ray-tracing and the Single Scattering Geant4 simulation, after normalising for the different efficiency. The two distributions, as shown in Fig. 4, are comparable.

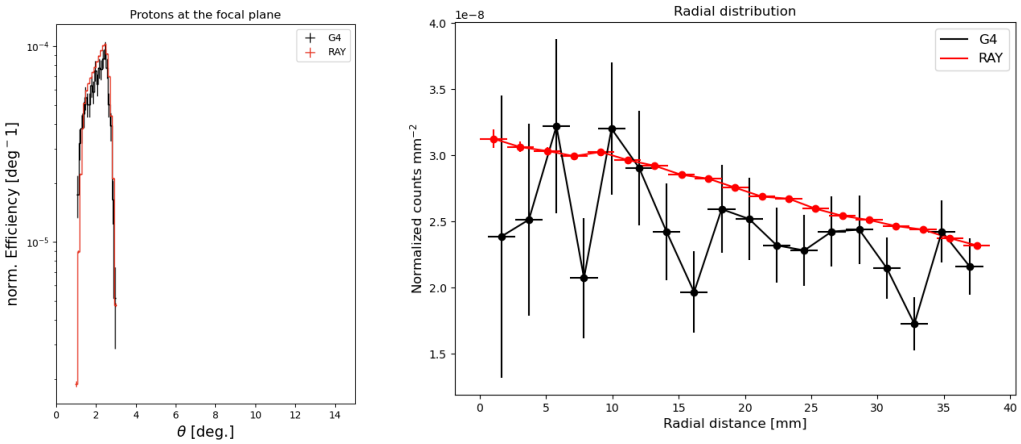

Figure 4: Comparison of the angular (left) and radial (right) distribution, after applying the factor 2 normalization in efficiency, between the Geant4 and ray-tracing simulation of the proton scattering at the XMM mirror for an input proton energy of 50 keV.

Two independent simulation frameworks, using different models for the physics interaction, provide similar angular and spatial distributions, but with a different normalization factor in the effective area, hence there is no need to build two simulation pipelines. While we consider this factor 2 discrepancy to provide the level of confidence to rely on when using the proton response files because of systematics in the proton scattering simulation accuracy, we selected the Geant4 simulation as the reference one to build the end-to-end simulation. The reasons are the followings:

- in the work of [12] both the elastic Remizovich and the Single Scattering models were compared against eROSITA scattering measurements and the Single Scattering predicted efficiency resulted closer to the laboratory data;
- the new Remizovich non-elastic approximation is an analytical expression obtained from modelling the laboratory experiment that covered a limited set of input energies and angles;

- in the Geant4 simulation, the Single Scattering uses theory-based cross-sections simulating every single collision[3] and the comparison against measurements was obtained using the physics list out-of-the-box without any adaptation.

1.4 Geant4 proton attenuation simulation (Task 1.4)

The focal plane assembly (FPA) surrounding the three EPIC cameras is the same. The main components of the Geant4 mass model of the EPIC FPA are, in addition to the cameras, the optical filters, the radiation shielding baffle, an Aluminum alloy baffle about 60 cm long placed at the top of the filter wheel, and surrounding structures modelled by a Titanium forward proton shield, 100 mm long (Fig. 5, left panel). While the presence of the radiation shielding is fundamental in reducing the non-focused particle-induced background (e.g., induced by galactic cosmic rays), in case of protons entering the field of view the secondary scattering at the baffle inner surface can potentially increase the background rate (see Sect. 5).

From top to bottom, we first encounter the Al proton shield (in grey) then the filter, the Ti forward proton shield (in yellow), and finally the camera at the focal plane. The figure also shows the entrance to the focal plane instruments (the door, in light green) and the filter wheel (in orange), which we did not simulate. We simply added a further Al truncated cone connecting the two proton shields, to simulate a closed environment and to avoid the dispersion of protons. The box surrounding the focal plane assembly is indicative to the reader and was not simulated.

The filter wheel is equipped with three different optical blocking filters [2] to reduce contamination from IR, visible and UV light collected in the field of view. With a diameter of 76 mm and placed at 10 cm from the focal plane, the observer can select among two thin filters, one medium filter and one thick filter (Table 2).

XMM-Newton optical filters

Filter	Layer 1	Layer 2	Layer 3
thin	Al (0.04 μm)	Pl (0.16 μm)	
medium	Al (0.08 μm)	Pl (0.16 μm)	
thick	Tin (0.045 μm)	Al (0.11 μm)	PP (0.33 μm)

Table 2: The composition and thickness of the optical blocking filters. The layer numbering starts at the mirror side.

1.4.1 MOS focal plane assembly

The MOS camera is composed by 7 front-illuminated CCDs operating from 0.5 to 12 keV. Each CCD is divided into 600 × 600 pixels, each with an area of 40 × 40 µm. The central CCD is at the focal point on the optical axis of the telescope, while the others are at a distance of 4.5 mm towards the mirror, to approximately reproduce the focal plane curvature. Each CCD has a 300 µm-wide dead region on three sides. They are rotated and disposed in order to cover the dead sides as much as possible, to maximize the exposed area. An Aluminum ring, 100 µm thick, is placed on top the CCDs to represent the camera metalwork limiting the field of view to 62 mm of diameter. The Geant4 model of the MOS CCDs is shown in Figure 5, right panel.

[3] Geant4 Physics Reference Manual v10.4

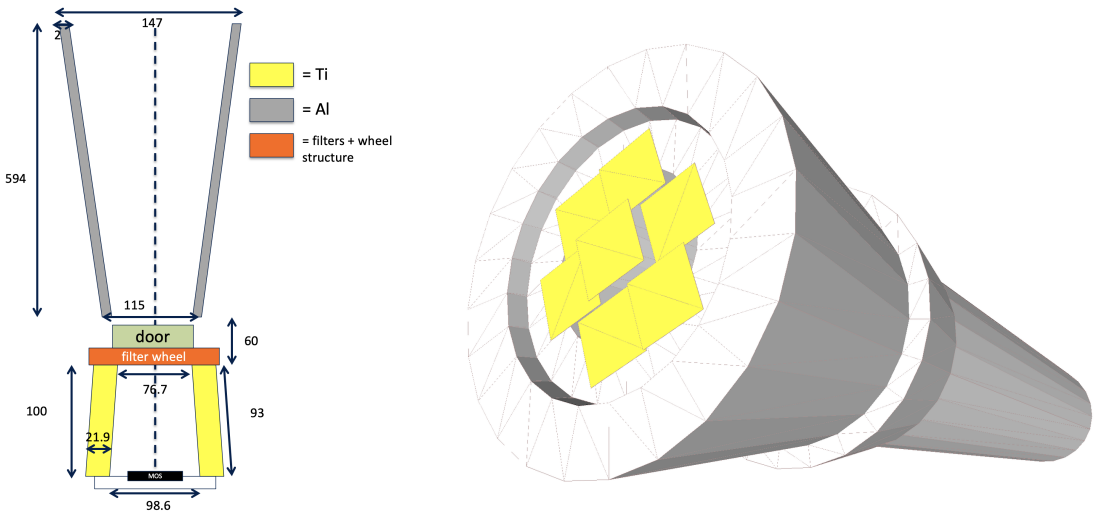

Figure 5: Schematic view of the XMM-Newton focal plane assembly geometry (left) and the respective bottom view of the Geant4 mass model, with highlighted in yellow the MOS CCDs.

The MOS conventional 3-phase front-illumination device is characterised by an open electrode structure [20] where one of the electrodes was partially etched, i.e. holes were cut through it, to increase the X-ray detection efficiency at low energies. The resulting device structure [21, 22] is divided into a 60% portion covered by the standard closed electrode structure, composed by a layer of Si (0.3 µm thick) and SiO2 (0.75 µm thick), and a 40% area of open electrode with only 0.085 µm of SiO2. The depletion region, made of Silicon, is 37 µm thick. Fig. 6 (left panel) shows a not in scale schema of the pixel geometry implemented in Geant4. The X-ray detection efficiency generated by the MOS CCD pixels was measured on-ground by sampling different positions of the array [21]. The resulting mean pixel X-ray response is compared in Fig. 6 (right panel) to the Geant4 simulation of the MOS quantum efficiency obtained by illuminating the array with a uniform photon beam from 0.2 to 10 keV. The two curves are in very good agreement above 0.5 keV, with residuals within some percentage. Towards lower energies we find a degradation in the accuracy that reaches 20% at the low energy threshold. Since the work of [21] does not include uncertainties in the curve, it is difficult to explain the source of the discrepancy. However, the general agreement well within 20% positively verifies the Geant4 implementation of the MOS camera, a key factor in correctly estimating the proton energy losses.

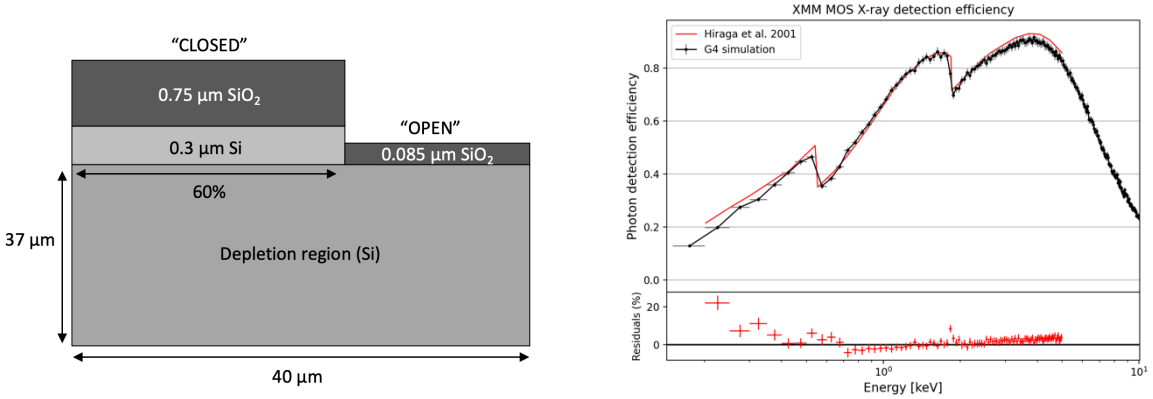

Figure 6: (left) Schematic side view, not in scale, of the MOS pixel geometry implemented in the simulation, with the open and closed electrode structure on top of the depletion region covering 60% and 40% of the pixel area respectively. (right) Comparison of the measured (red line) and simulated (black line) MOS X-ray detection efficiency (the error bars refer to the simulation statistical uncertainty).

The simulation of the proton transmission efficiency is obtained by randomly simulating protons within a circle with a diameter of 76 mm (equal to the filters), centered on the optical axis of the telescope and perpendicular to it. Proton energies are randomly generated in the range 2–300 keV, and then selected in the analysis in input bins of 1 keV to evaluate the transmission efficiency. The latter is defined as the number of protons that deposit energy within the MOS energy range over the total number of simulated protons within the bin. From the transmission efficiencies of all the simulated detectors we define a common input energy range of 2 - 300 keV. While the instrument proton detection efficiency is very low above 200 keV, we extended the upper limit to 300 keV to test the effect of secondary scattering with the baffle and surrounding volumes.

The MOS result is shown in Fig. 7, where two peaks in the transmission efficiency appear, one centered at ~ 35 keV if protons cross the open electrode, and one centered at ~ 160 keV if they encounter instead the thicker closed electrode. For the analytical computation, proton stopping powers reported by NIST[4] were used for all of the materials involved. The stopping power was interpolated using Mathematica[5], and the energy loss after each layer of the filters and the electrodes was calculated as a function of their thickness. As a result, we obtained the energy of the proton when impacting on the sensitive layer of the MOS detector, as a function of the incident energy and the thickness of each layer crossed by the particle, that were left as free controllable parameters in the computation to allow probing different configurations. The analytical computation defines an energy range where protons are able, according to the tabulated stopping power, to reach the MOS pixels without losing all their energy. Not only the two peaks predicted by the Geant4 simulations are confirmed by the tabulated stopping power, but the energy ranges are also consistent if we consider the uncertainties introduced by the angular spread and the complex geometry of the pixels.

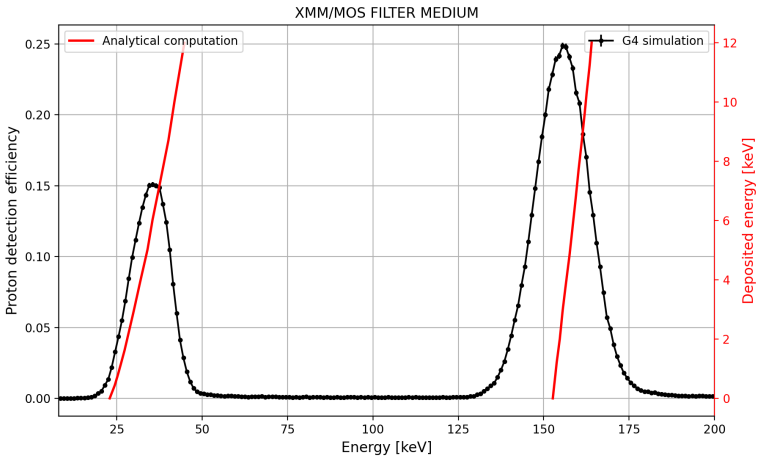

Figure 7: Simulated, in black, proton transmission efficiency in the 8 – 200 keV energy range for the MOS and medium filter. The analytical computation based on tabulated NIST proton stopping power predicts the proton energy range for which the MOS is likely to register a count, with an energy labelled by the red y-axis.

[4] https://physics.nist.gov/PhysRefData/Star/Text/PSTAR.html

[5] Wolfram Research, Inc., Mathematica, Version 9.0, Champaign, IL (2012)

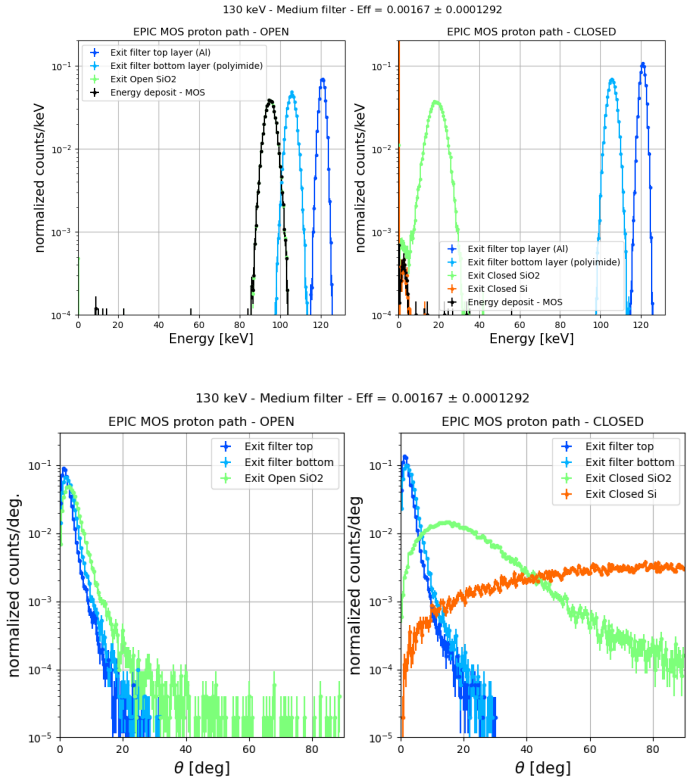

Figure 8: Energy and angular distribution of the protons, for an input energy of 35 keV, exiting each layer of the medium filter and electrode structure, open in the left panel and closed in the right panel.

The proton energy and angular distribution at the exit of each layer was analyzed for a set of energies to verify the analysis pipeline processing the FPA simulation. Fig. 8 shows the result for a 35 keV input proton beam, where the transmission efficiency low energy peak is centered. About 20 keV are lost in the medium filter, and while the closed electrode absorbs the remaining energy, if protons reach the open structure their final energy falls in the 5–10 keV band. The proton direction spread, defined as the angle from the telescope axis, increases linearly while crossing the passive layers, and the medium filter alone introduces a $5° - 10°$ medium shift. This angular spread impacts the number of protons that are able to reach the detector, and the height of the filter from the focal plane is a parameter that can modify the soft proton-induced background. The front-illuminated device drastically increases the spread, and the protons lose the memory of their incident direction.

The successful verification of the Geant4 simulation of the EPIC optical filters and MOS electrode structure, by comparing both tabulated results and laboratory measurements, was a mandatory stepstone in the overall XMM end-to-end simulation. The resulting MOS detection efficiency for the three filters is shown in Fig. 9.

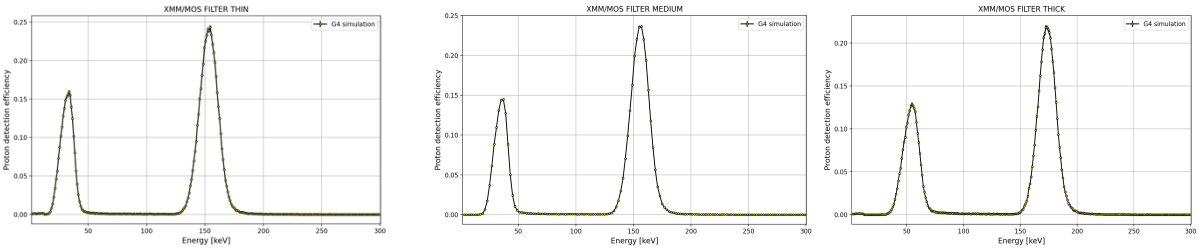

Figure 9: MOS FPA proton detection efficiency for a thin (left), medium (center) and thick (right) filter

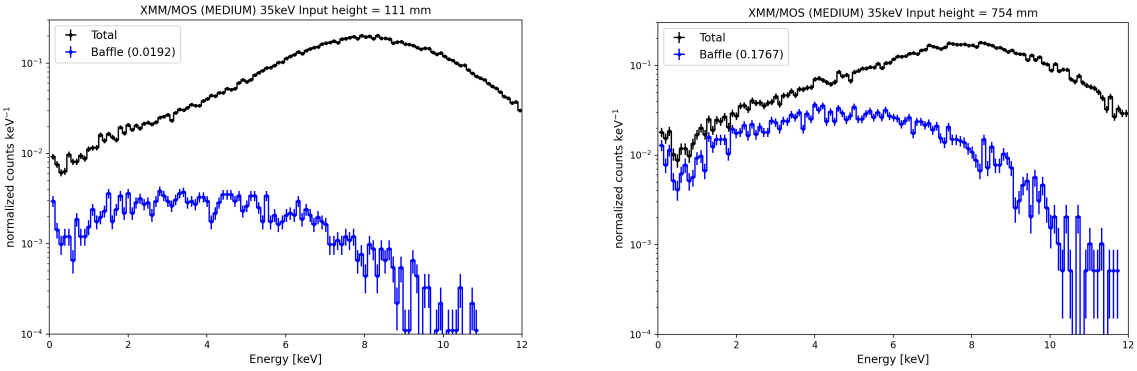

Figure 10: Soft proton induced X-ray spectra, for an incident energy of 35 keV, obtained extracting the mirror simulation proton list at a height of 111 mm (at the optical filter, left panel) and 754 mm (the baffle entrance, right panel). Protons interacting with the baffle surface before generating a count on the MOS are highlighted in blue, and their fraction concerning the total is reported in the legend.

The impact of the proton shield in scattering soft protons was tested with the MOS camera as a use case, by extracting the output of the mirror simulation at two heights: 754 mm, the baffle entrance, and 111 mm, at the optical filter. Using the baffle flag of data level 1 (Sect. 3.1), we can estimate the fraction of protons that scatter with the focal plane baffle before generating the background event. The result is shown in Fig. 10. The fraction of protons that scatter with the radiation shielding increases from 2% for a height of 111 mm (left) to ~ 18% for the 754 mm case (right). Protons scattering with the baffle surface lose energy and increase the low energy tail of the spectrum. This effect is visible in the plot, softening the background spectral distribution.

For this reason, in the XMM FPA simulation protons were generated at the top of the baffle. We note, however that when taking into account the whole input energy range and considering the general uncertainties of the simulation set-up, the final background flux generated by two prototypes of the proton response files, obtained at 754 and 111 mm input protons, the impact of the baffle is no longer visible (Fig. 11). The statistical uncertainties are instead much more improved if protons are generated at the optical filters. For this reason, in the WFI FPA simulation (see Sect. 2.4) the protons were simulated at the filter wheel height, i.e. we have chosen to increase the statistics while neglecting the impact of secondary scattering.

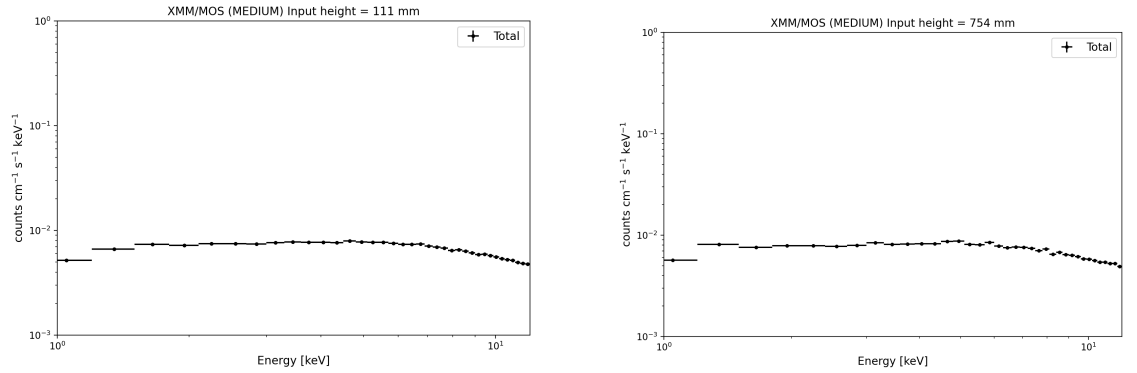

Figure 11: Soft proton induced background flux obtained simulating protons at the optical filter (left) and baffle entrance (right).

In the Geant4 FPA simulation, the output of the mirror simulation is used as input (see Sect. 3.2 for details) and the energy deposits in the depleted region of the pixels are stored in output files, with their position and

an associated flag if the proton interacts with the baffle. The raw simulation output is then reconstructed into a list of counts, where all the energy deposits within the same pixel in the same event are summed up. A count is a total energy deposit within the MOS energy range (0.2 - 12 keV). Fig. 12 (left) shows the count map produced by a 35 keV proton entering the mirror.

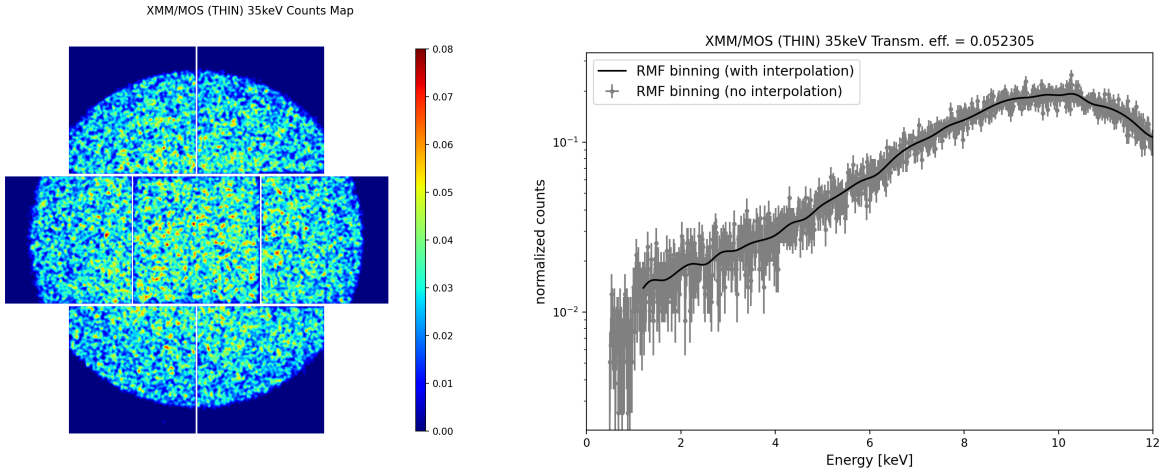

Figure 12: MOS (medium filter) counts map (left) and interpolation of the spectral distribution (right) for an input energy of 35 keV at the mirror entrance.

The counts are first binned using the X-ray RMF channels (see Sect. 3.1), as shown in grey in Fig. 12 (right). Statistical errors dominate the plot, and the energy distribution cannot be directly stored in the proton RMF.

The adopted solution was to rebin and interpolate the histogram, the black curve of Fig 12 (right), and use the interpolation function to fill the RMF. If the number of counts was not enough to produce a histogram in the first place, a constant was used along the covered energy range. This method allowed to automatically generate the RMF model for all the input energies despite the limited statistics, but it also caused some caveats in the proton response file usage. The interpolation function produces artefacts at the border of the energy range, in particular when the count number is low. We tested (see Sect. 3.3) each response matrix against a standard simulation - where no artefacts are present since there is no interpolation - and defined a validity energy range for the use of the response files from this comparison.

We also note the cut in the MOS energy spectrum at about 1 keV (Fig. 12, right). Since the accuracy of the Geant4 modelling of the proton stopping power degrades below 1 keV (20% at 1 keV reported in the Geant4 Physics Reference Manual[6]), the simulated proton efficiency at the detector also features a reduction at low energy that is not physical but caused by internal limits in the Geant4 physics model. For this reason, the energy redistribution is modelled from 1 keV to the upper threshold of the instrument X-ray RMF.

1.4.2 PN focal plane assembly

The PN camera [2] is instead back-illuminated, composed of four quadrants each having three CCDs with 200 × 64 pixels, with a pixel size of 150×150 μm and a total imaging area of 6×6 cm. The fully depleted Silicon thickness is 300 μm. Being back-illuminated, no read-out devices are present in front of the PN

[6] https://geant4-userdoc.web.cern.ch/UsersGuides/PhysicsReferenceManual/BackupVersions/V10.4/html/index.html

camera, simplifying its Geant4 implementation. In addition, no metalwork is placed on top of the camera and contrary to the MOS, all the CCD area is exposed to the soft proton flux.

The PN proton transmission efficiency for the three filters is shown in Fig. 13. We note that with the lack of the electrode multi-structure on top, there is only one peak in the efficiency.

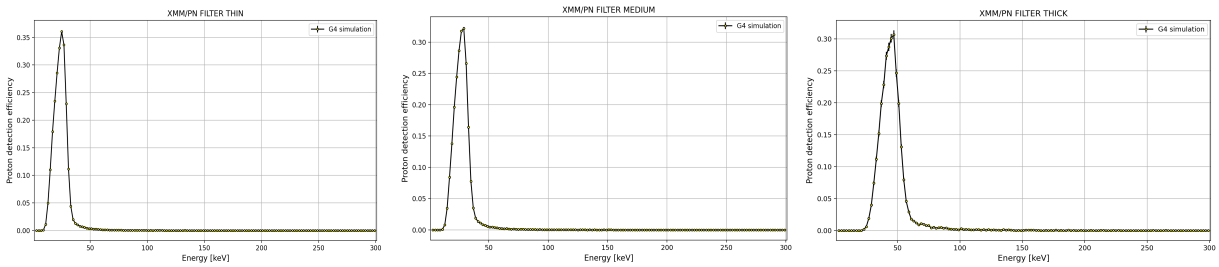

Figure 13: PN FPA proton detection efficiency for a thin (left), medium (center) and thick (right) filter.

The PN counts map, in the 0.2 - 20 keV energy range, is shown in Fig 14 (left) for an input proton energy of 35 keV. The RMF for the PN followed the same method of the MOS, with the energy spectrum first re-binned and interpolated, and then the interpolation function was used to fill the same channels of the X-ray RMF (Fig. 14, right).

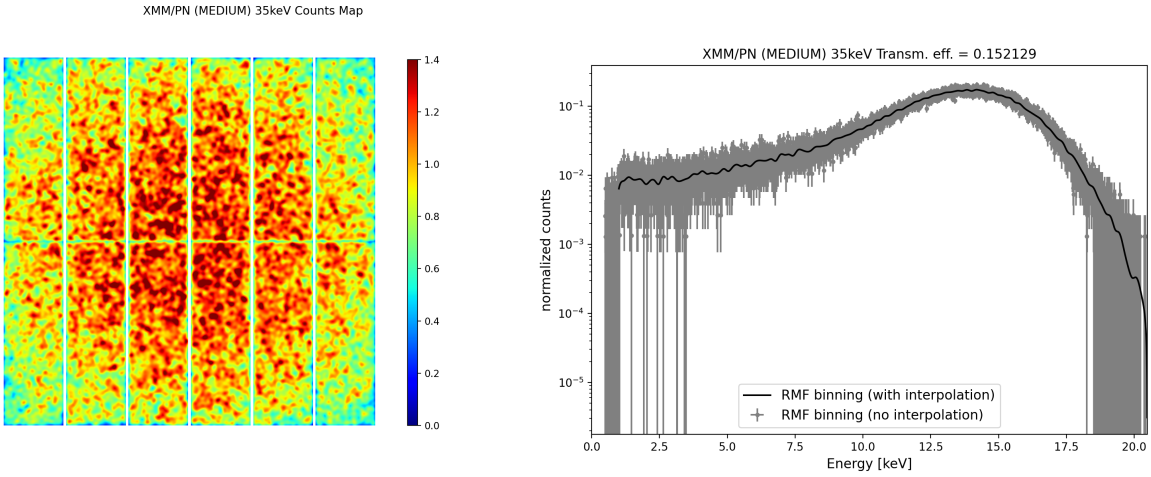

Figure 14: PN (medium filter) counts map (left) and interpolation of the spectral distribution (right) for an input energy of 35 keV at the mirror entrance.

2. ATHENA proton response matrix design (Task 2)

The ATHENA space telescope is the future ESA L-class X-ray mission [23], designed to address the Cosmic Vision "The Hot and Energetic Universe" science theme. With a planned launch in the 2030s in an L1 orbit, ATHENA will carry an X-ray modular mirror based on Silicon Pore Optics (SPO) technology with a focal length of 12 m and an unprecedented effective area of 1.4 m^2 at 1 keV. Two instruments populate the focal plane, covering the soft < 15 keV energy range: a Wide Field Imager (WFI [24]) for wide field imaging and spectroscopy and an X-ray Integral Field Unit (X-IFU [25]) for fine X-ray spectroscopy.

Geant4 simulations of the soft proton-induced background at both detectors [26, 27] have proved that soft protons threaten the achievement of the ATHENA scientific requirements. For this reason, a magnetic diverter has been designed to shield the focal plane from charged particles entering the field of view, and simulations for the focused background drove its specifications.

Because of the complexity and large diameter of the mirror, both Geant4 and ray-tracing simulations of the proton scattering effect require significant CPU running times to get a minimum statistical level, so testing different input models and exploring different requirements for the diverter is practically impossible. The ATHENA proton response files will provide fast evaluations of the soft proton-induced background level - without the magnetic diverter - to optimize the diverter design and better characterize the focused background.

2.1 Geant4 ATHENA soft proton scattering (Task 2.1)

The Athena SPO proton scattering efficiency was extensively evaluated [27] during the ESA AREMBES project with independent mirror models built using Geant4 and ray-tracing simulation frameworks, with a systematic difference in the efficiency of about 20% using the same scattering model. In the meantime, a new SPO design was released [28] with a different mirror module layout and a rib pitch of 2.3 mm. The Geant4 mass model delivered by the AREMBES project [10] was updated to a rib pitch of 2.3 mm according to the most recent SPO design. The effect of the new layout was introduced as a normalization factor in the ARF based on the results obtained with the ray-tracing simulator (Sect. 2.2). The geometry uses a truncated cone to emulate the paraboloid and hyperboloid stacks of the mirror modules, with a total of modular 15 rows built in the Geant4 code [Fig. 15]. No coating is applied to the reflecting surface because simulations performed in the past indicated a difference in the scattering efficiency by a few percent. The Single Scattering model is used to model the proton interaction with the mirror surface.

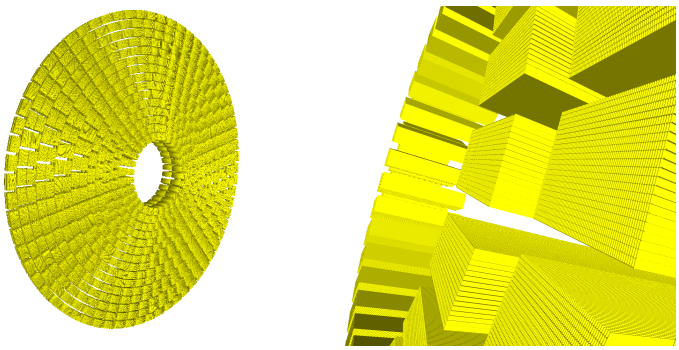

Figure 15: Geant4 mass model of the updated ATHENA SPO.

2.2 Ray-tracing ATHENA soft proton scattering (Task 2.2)

Th optics are simulated as concentric shells (one for each plate) with pores and multiple reflections inside pores are not considered. Both the new rib pitch and mirror layout were included in the updated simulation. The proton scattering physics interaction uses the Remizovich model in non-elastic approximation. The new mirror geometry has been implemented in the code and verified by comparing the on-axis X-ray photon transmission from a point source with the X-ray effective area and vignetting presented in the SPO ESA report [28]. Fig. 16 shows the agreement between the current ray-tracing simulation and the SPO performance.

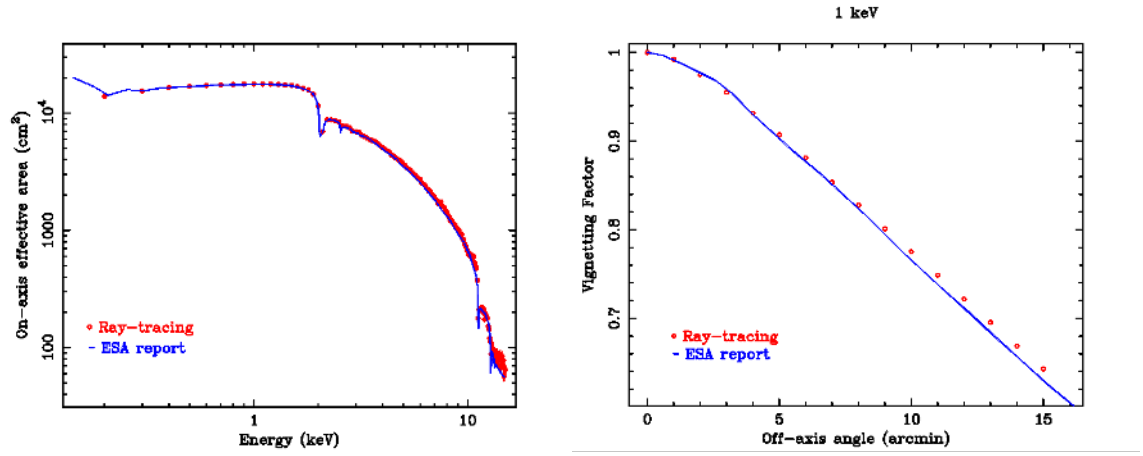

Figure 16: (left) On-axis effective area for a point source as a function of the photon energy: the red dots are values obtained from the ray-tracing, and the blue line is the curve presented in the ESA report. (right) The vignetting factor for 1 keV input photons as a function of the input angles: the red dots are values obtained from the ray-tracing, and the blue line is the curve presented in the ESA report.

We simulated the proton flux at the focal plane, defined as a circular region with a radius of 10 cm, using the Geant4 (Single Scattering) and Ray-tracing (Remizovich) simulators. We compared the spectral and radial distributions, and the transmission factor T defined as:

$$T = \frac{N_{out} \times \Omega_{in} \times A_{SPO}}{N_{in} \times 4\pi \times A_{FP}}$$

where N_{in} and N_{out} are the input and exiting protons, Ω_{in} is the input cone solid angle, A_{SPO} and A_{FP} are the SPO surface and the 10 cm radius focal plane respectively.

With the new rib pitch of 2.3 mm, we obtain:

- Geant4 T (old layout): 4.6×10^{-5};
- Ray-tracing T:
  - old layout: 9.9×10^{-5} (2x Geant4);
  - new layout: 1.5×10^{-4} (3x Geant4, given by the 2x factor for the different physics model and the 1.5x factor for the layout).

In terms of efficiency, the new mirror layout increments the proton effective area by a 1.5 factor, while keeping the same spectral and angular distribution. Fig 17 shows the proton spectra obtained at the focal plane, with the left panel referring to the new layout and the right panel to the old one. Fig. 18 computes for a set of radial annuli from the center of the focal plane the mean proton angle w.r.t. the telescope axis. Thanks to this consistency, a 1.5 incremental factor was added to the Geant4 ARF files without the need to build a new Geant4 mass model of the ATHENA SPO.

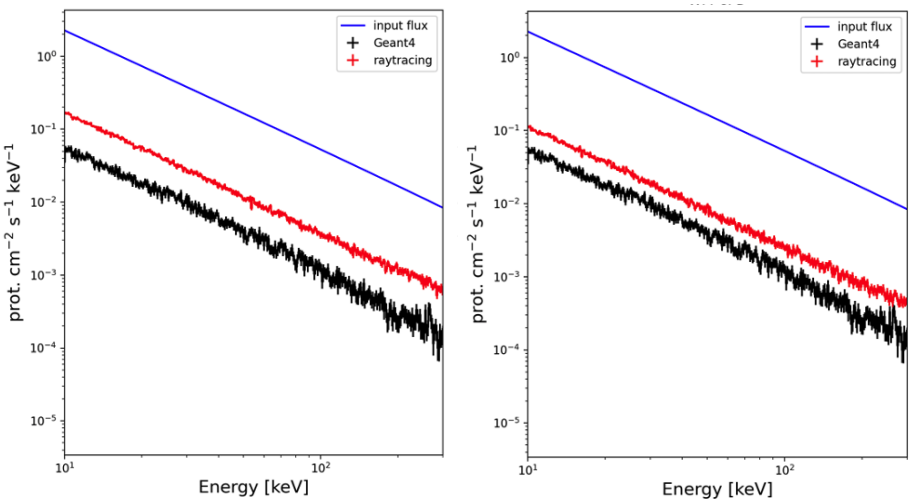

Figure 17: The Geant4 and ray-tracing simulated proton spectra at the 10 cm radius focal plane after scattering with the SPO. From left to right, the ray-tracing uses the new and old SPO mirror module layout.

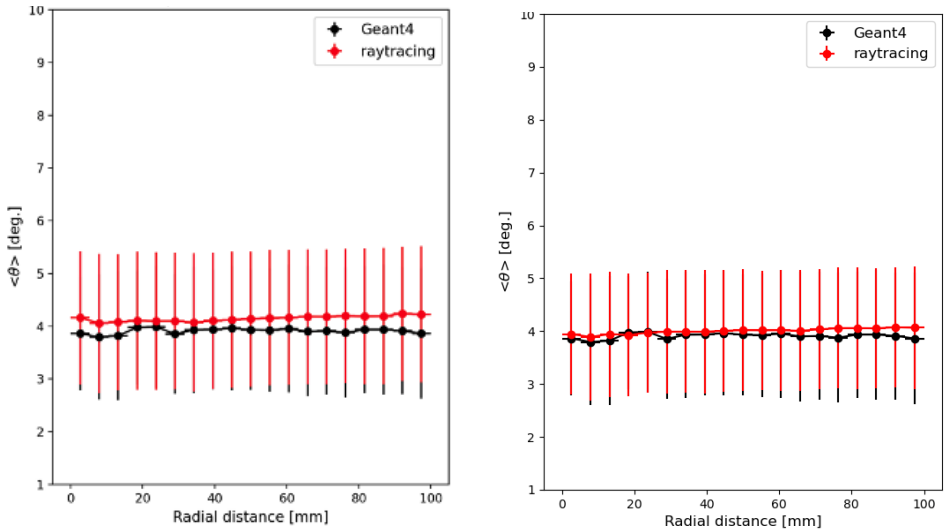

Figure 18: The Geant4 and ray-tracing simulated mean proton angle along the radial distribution at the 10 cm radius focal plane after scattering with the SPO. From left to right, the ray-tracing uses the new and old SPO mirror module layout.

2.3 Geant4 X-IFU proton scattering simulation (Task 2.3)

The Geant4 mass model of the X-IFU FPA was provided by the ATHENA X-IFU instrument background working group and a detailed description can be found in [29]. The mass model includes the set of fixed thermal filters placed within the cryostat aperture cylinder at the top of the detector according to the latest design. We will refer to the X-IFU filters as Optical Blocking Filters (OBF) for consistency with the WFI design. The proton detection efficiency within the 0.2 - 12.5 keV energy range is shown in Fig. 19. We note that a long tail extends to the energy upper limit and that at 300 keV there is still a non-negligible fraction of protons that is detected by the X-IFU, even if with an efficiency more than 10 times lower than the peak. This is likely caused by multiple secondary scattering within the aperture cylinder, with protons losing energy at each scattering with the inner surface.

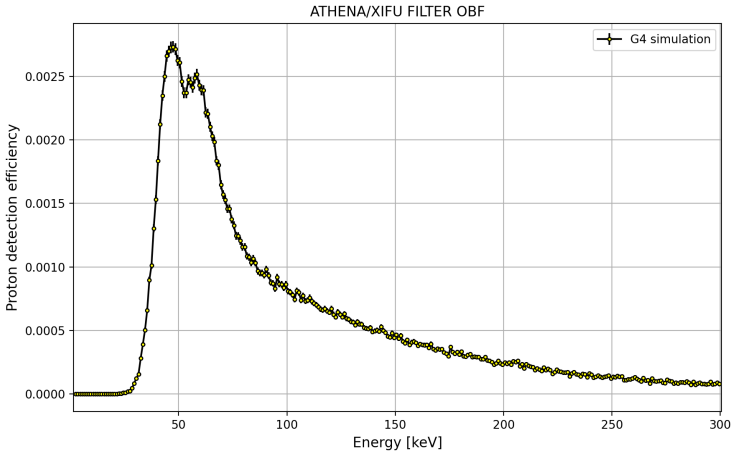

Figure 19: X-IFU FPA proton detection efficiency.

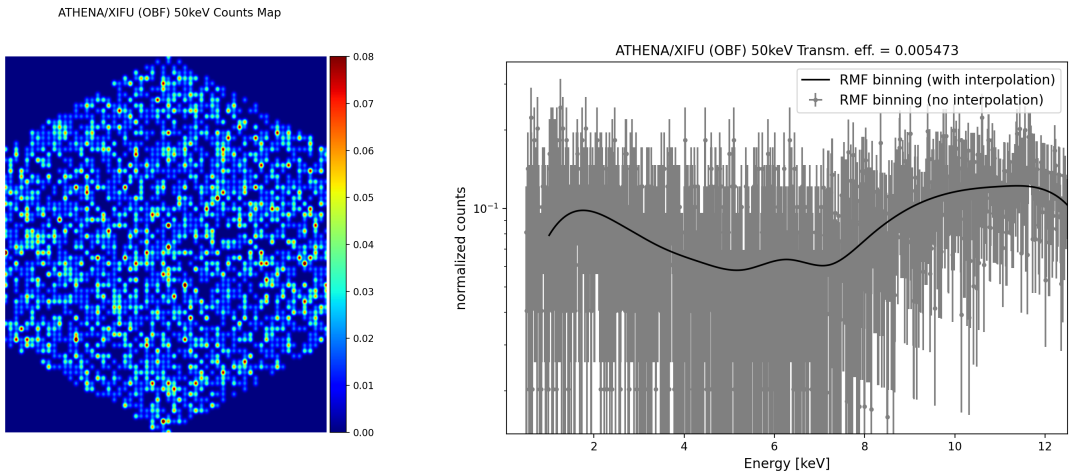

Figure 20: X-IFU counts map (left) and interpolation of the spectral distribution (right) for an input energy of 50 keV at the mirror entrance.

The input protons used for the FPA are extracted at the aperture cylinder entrance at 388 mm from the detector. The proton lists were first modelled in angular and energy distribution and then randomly generated for the EPIC simulation.

The same event reconstruction described for the MOS in Sect. 1.4.1 was used for the ATHENA instruments. The X-IFU counts map, in the 0.2 - 12.5 keV energy range, is shown in Fig 20 (left) for an input proton energy of 50 keV. The RMF for the X-IFU uses the same pipeline of XMM, with the energy spectrum first re-binned and interpolated, and then the interpolation function filling a reduced set of channels (Fig. 20, right) as described in Sect. 3.1.

2.4 Geant4 WFI proton scattering simulation (Task 2.4)

The WFI Geant4 mass model, built for the WFI instrument background group simulations [27], includes:

- The wide field detector itself, composed of four pixelated quadrants each with 512×512, 130×130 μm^2 side pixels, with a thickness of the Si sensor of 450 μm;
- The fixed on-chip filter covering the pixels of the four quadrants and composed, from top to bottom, of 90 nm of aluminum (Al), 30 nm of silicon nitride (Si3N4), and 20 nm of silicon oxide (SiO2);
- The squared 17×17 cm^2 Optical Blocking Filter on the filter wheel composed from top to bottom of 30 nm of Al and 150 nm of Kapton (polyimide). This filter is optional depending on the wheel position.

A squared Aluminum baffle is placed on top of the WFI. Given that the MOS proton response files are not affected, within the uncertainties, by the baffle secondary scattering we decided to extract the proton at the filter wheel height, 10 cm, and neglecting the effect of the baffle. This allowed us to increment the statistics and to better model the energy redistribution. The proton detection efficiency within the 0.2 - 15 keV energy range is shown in Fig. 21 with and without the OBF.

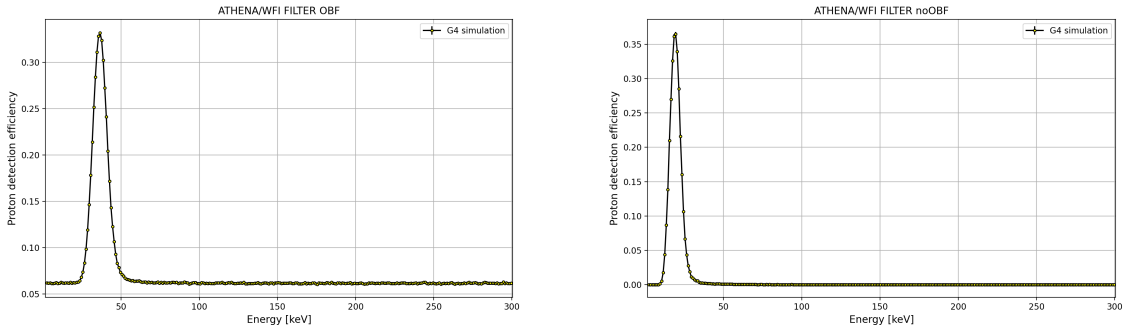

Figure 21: WFI proton detection efficiency with (left) and without (right) the OBF.

The event reconstruction is the same as the previous instruments. The WFI counts map, in the 0.2 - 15 keV energy range, is shown in Fig 22 (left) for an input proton energy of 50 keV. The RMF for the WFI uses the same pipeline of XMM, with the energy spectrum first re-binned and interpolated, and then the interpolation function filling the X-ray RMF channels (Fig. 22, right) as described in Sect. 3.1.

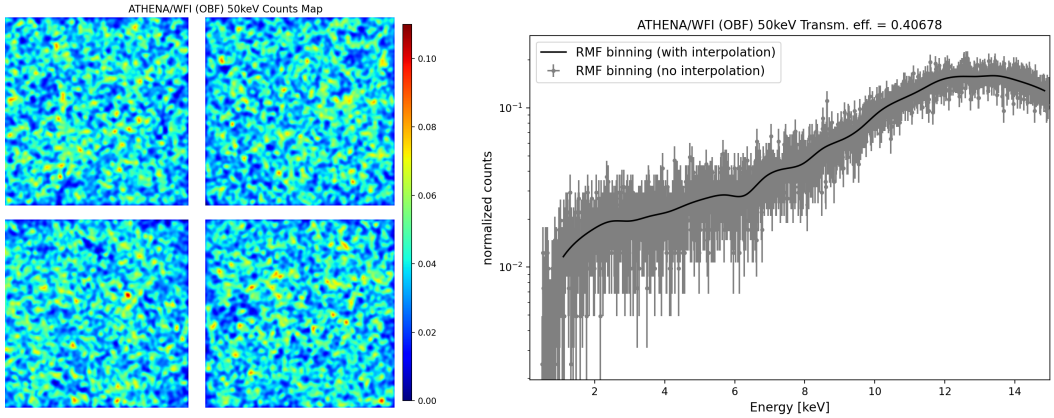

Figure 22: WFI counts map (left) and interpolation of the spectral distribution (right) for an input energy of 50 keV at the mirror entrance.

3. Data formatting, verification and validation (Task 3)

3.1 Data input formatting (Task 3.1)

The proton response files are composed by a Redistribution Matrix File (RMF) mapping the proton energy space (from few to hundreds of keV) into detector pulse heights and an Auxiliary Response File (ARF) collecting the grasp of the optics, the filter transmission efficiency and the detector quantum efficiency. The files are formatted according to the NASA OGIP (Office of Guest Investigators Program) calibration database (caldb) format, and it consist into an RMF and ARF file in FITS (Flexible Image Transport System) format. Any X-ray data analysis tool available to the X-ray astronomy community and compliant with the NASA caldb format can be used to simulate the soft proton induced background spectra, for any given condition of the orbit proton environment without the need to run again the simulation pipeline. We chose the NASA *Xspec*[7] fitting package for the verification and validation results presented in Sect. 3.3 and 3.4.

The energy distribution is binned according to the respective instrument X-ray channels, except for the X-IFU. Because of the smaller aperture and detection area, its simulation was the one that suffered the most from the limited statistics and using the original energy resolution, the smallest among the simulated detectors, was practically impossible. A binning factor of 25 was instead used.

- The EPIC cameras[8]:
  - MOS: a total of 800 channels, an energy width of 15 eV and energy boundaries of 0 – 12 keV.
  - PN: a total of 4096 channels, a mean energy width of 5 eV and energy boundaries of 0 - 20 keV.
- The ATHENA X-ray instruments[9,10]:
  - X-IFU: a total of 1196 channels, an increasing energy width from about 5 eV to about 30 eV and energy boundaries of 0.06116 - 12.49961 keV.
  - WFI: a total of 1485 channels, an energy width of 10 eV and energy boundaries of 0.15 - 15 keV.

3.2 XMM-Newton and ATHENA proton response matrix (Task 3.2)

The simulation pipeline logical schema is shown in Fig. [23]. The mirror simulation is performed with two independent simulation frameworks based on ray-tracing and the Geant4 toolkit in order to verify the geometry and physics models and estimate potential systematic effects in their implementation. Since the two simulators give comparable angular and spatial distributions of the protons at the focal plane, with only a factor 2 difference in the proton flux affecting the grasp stored in the ARF file, only the output of the Geant4 simulator, in the form of an event list, storing energy and angular distribution of the protons at a given distance from the focal plane, is extracted and given as input to a Geant4 simulation of the FPA, including baffles, optical filters and the detectors. From the FPA simulation, we reconstruct the counts on the XMM-Newton and ATHENA detectors, applying a pattern flag, according to the instrument read-out

[7] https://heasarc.gsfc.nasa.gov/xanadu/xspec/

[8] https://www.cosmos.esa.int/web/xmm-newton/epic-response-files

[9] http://x-ifu-resources.irap.omp.eu/PUBLIC/RESPONSES/CC_CONFIGURATION/

[10] https://www.mpe.mpg.de/ATHENA-WFI/public/resources/responses/

configuration, and a baffle flag for the protons that interact with the radiation shielding before reaching the detector. The product of this processing stage is a data level 1 FITS file listing the count energy, position, pattern and baffle flags, one for each Geant4 simulation run of each input energy. In data level 2 we compute for each input energy the energy probability distribution in the instrument channels, normalized to 1, and the grasp. For X-ray photons, that are mono-directional, the response ARF file is the product of the effective area of the mirror, i.e. geometric area multiplied by the reflection efficiency, the filter transmission efficiency and the detector quantum efficiency. For the soft proton environment, we assume an isotropic distribution at the mirror entrance and the input aperture angle used in the simulation must be taken into account when computing the total transmission efficiency. The simulated grasp is the product of the system efficiency multiplied by the proton aperture solid angle at the mirror entrance, in units of cm^2 sr. The data level 2 files are then unified and formatted into the OGIP RMF and ARF response files. A different proton response will be produced for each combination of mirror simulator, optical filter type, and focal plane instrument.

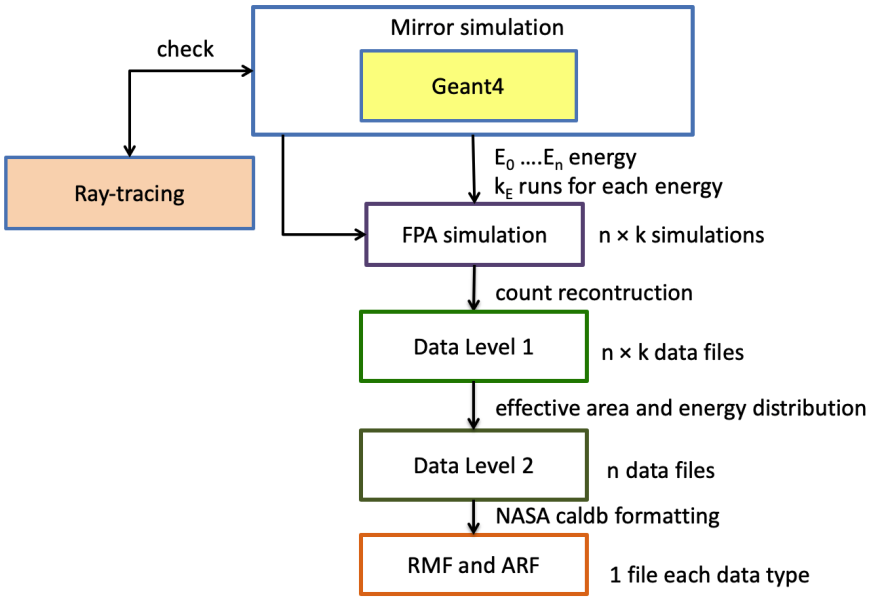

Figure 23: Logical schema of the software pipeline generating the response files.

The pattern analysis shows that 99.9% of the simulated counts has a pattern of 0, i.e. only one pixel triggered for each event, as in the in-flight focused non X-ray background. For this reason, all the proton response files were produced selecting only singles (PATTERN = 0 for the EPIC cameras). We note here that the PATTERN terminology was also used for ATHENA since its terminology and selection criteria are still unknown.

At first, we planned to connect the FPA to the mirror simulation by using the same proton list at the mirror output as input for the FPA simulation. This allows to reproduce the exact same angular, spatial and energy distribution. However, the CPU simulation time required to achieve a minimum statistical level to model the energy distribution turned out to be unfeasible (6 months for XMM, more than 1 year for ATHENA). The solution was to model the angular and energy distribution of the protons at the input of the FPA simulation and then exploit the Geant4 Monte Carlo generator to randomly sample the protons within the modelled distribution. There are several assumptions in this approach: (i) the protons are spatially uniform when reaching the FPA, (ii) the angular distribution is spatially uniform, (iii) there is no dependence among the proton energy, angle and the position. Selecting the MOS as a use case, we tested that at a height of 754

mm (the baffle entrance) both the assumptions (i) and (ii) can be considered valid, within the statistical uncertainties, as shown in Fig. 24 (for a 50 keV input proton energy).

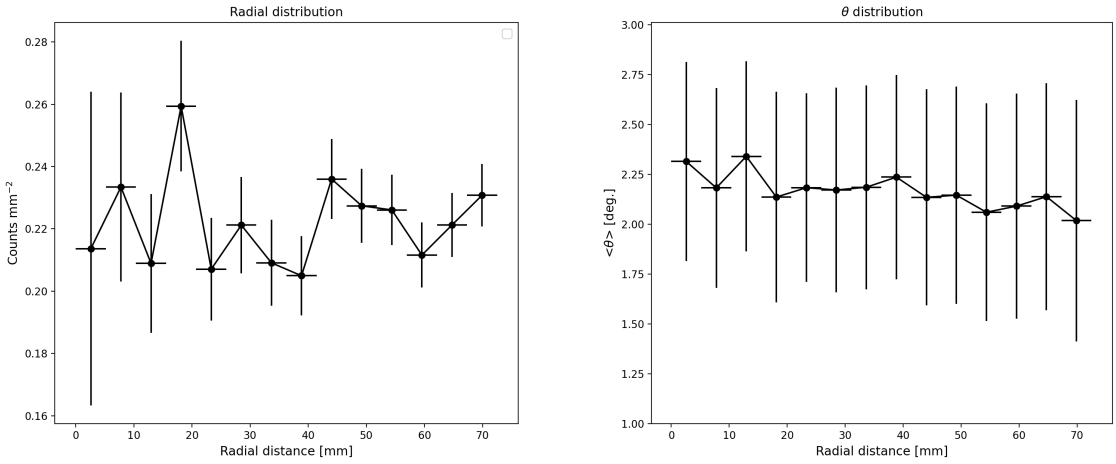

Figure 24: Radial distribution (left) and radial distribution of the mean angular distribution w.r.t. the normal (right) of the protons exiting the XMM mirror and entering the baffle at 754 mm from the MOS.

To test the third assumption, i.e. to assess that we did not introduce any biases in the approximations of the modelled proton distribution, we produced two simulated background spectra, one obtained with the proton list and one with the modelled distribution (Fig. 25). The resulting spectra are comparable, despite the limited statistics of the spectrum using the proton lists as input.

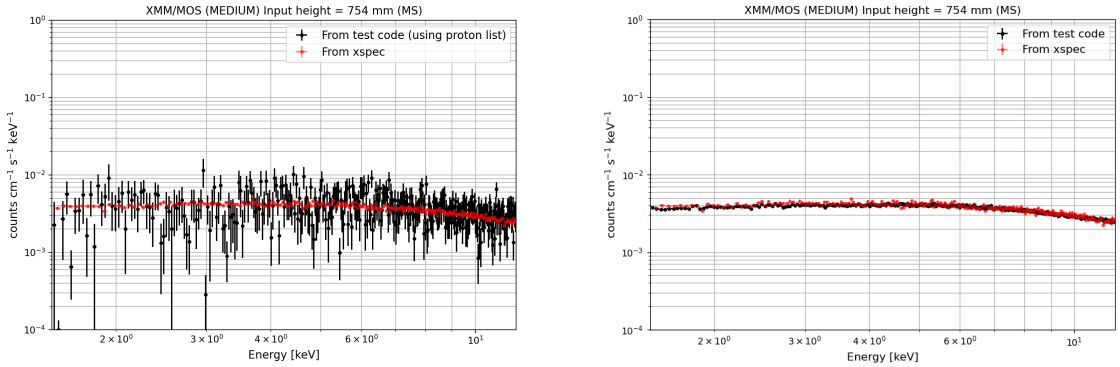

Figure 25: Comparison of simulated background spectra, in black, using proton lists (left) or models (right). The simulation obtained with the final proton response file is shown in red.

The resulting energy redistribution matrix, plotted as incident vs measured energy and stored in the RMF files, is shown in Fig 26 and 27 (medium filter for the EPIC cameras and with OBF for the WFI). For each input proton energy (Y-axis), the RMF stores the energy distribution detected by the instruments (X-axis) normalized to 1. The presence of the two peaks in the MOS transmission efficiency is clearly visible. The RMFs and ARFs files are averaged on the camera field of views.

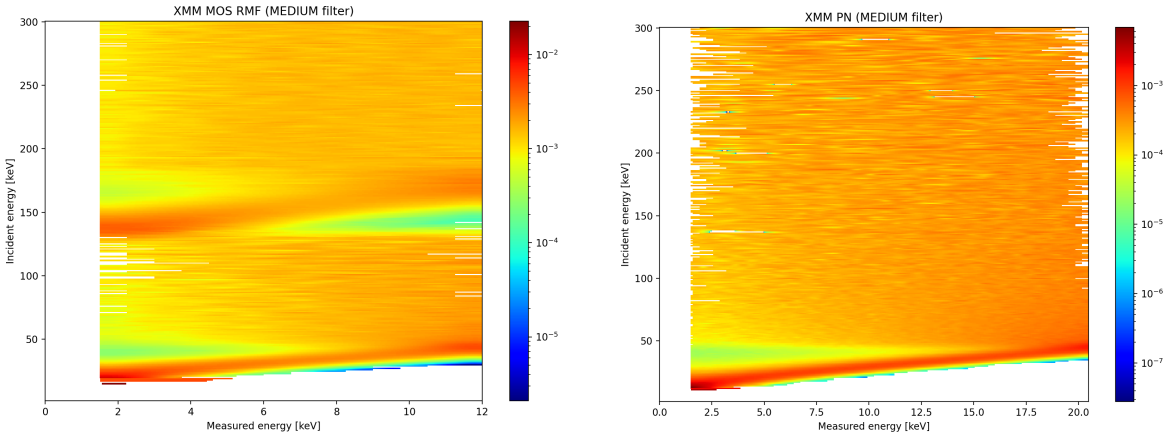

Figure 26: Plot of the RMF for the EPIC MOS and PN CCDs (medium filter

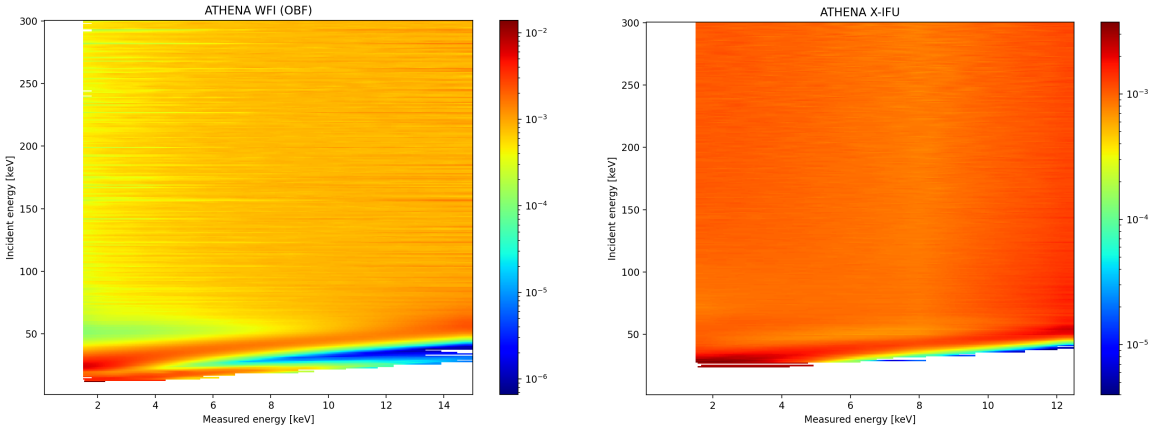

Figure 27: Plot of the RMF for the ATHENA WFI (with OBF) and X-IFU detectors.

The validity energy ranges, required to avoid artefacts by the interpolation model and defined by the comparison with standard simulations (see Sect 3.3) are:

- The EPIC cameras:
  - MOS: 1.5 - 11.5 keV
  - PN: 1.5 - 19.5 keV
- The ATHENA X-ray instruments:
  - X-IFU: 1.5 - 7 keV (the limited upper energy threshold is due to the lower statistics achieved in the X-IFU Geant4 simulations because of the intrinsic lower soft proton induced background flux)
  - WFI: 1.5 - 11.5 keV

The user should ignore the channels outside the validity ranges when performing their analysis.

Considering the 15-20% systematic uncertainty in the mirror simulation, the approximation (< 20%) introduced by sampling models of the proton list at the FPA input, and considering the factor 2 of difference between the Geant4 and ray-tracing simulated effective area, we assign a total uncertainty of 50% to the simulations obtained with the proton response files, to which the user must sum the errors in the input models.

3.3 Verification of the XMM-Newton and ATHENA response files (Task 3.3)

The verification of the proton response files consisted in checking their technical correctness by simulating the X-ray background spectrum with *Xspec* using the proton response files, as a general user would do, and in parallel using the L1 data files that store a list of counts for each input energy, to obtain a "standard" simulation where a model is used as input at the mirror entrance and the background is obtained by collecting the counts at the detector.

We chose as input models two proton spectral distributions based on in-flight measurements and representative of very different environments: the interplanetary solar wind (SW) that spacecrafts encounter when operating outside the Earth's magnetosphere, and the magnetosheath (MS), a plasma regime of the magnetosphere lying behind the bow shock boundary layer in the magnetotail up to the L2 region. The protons models for the MS and SW were extracted in [26] to simulate the ATHENA soft proton-induced background in L1 and L2. They refer to an active state of the magnetosphere and the maximum flux encountered in 90% of the operational time. Given the highly elliptical orbit of XMM-Newton, crossing both regions inside and outside the magnetosphere, these models can also represent the soft proton fluxes potentially producing the XMM's flares. The input proton models are shown in Fig. 28. While the uncertainties for the MS model are based on the AREMBES reported uncertainties, for the SW, for which more extended observations were available, we assumed a standard 20%. We must note that both models were produced from observations starting at about 50 keV (47 keV for the SW and 58 keV for the MS) and then extrapolated to lower energies. No actual measurements are available in the very soft proton regime.

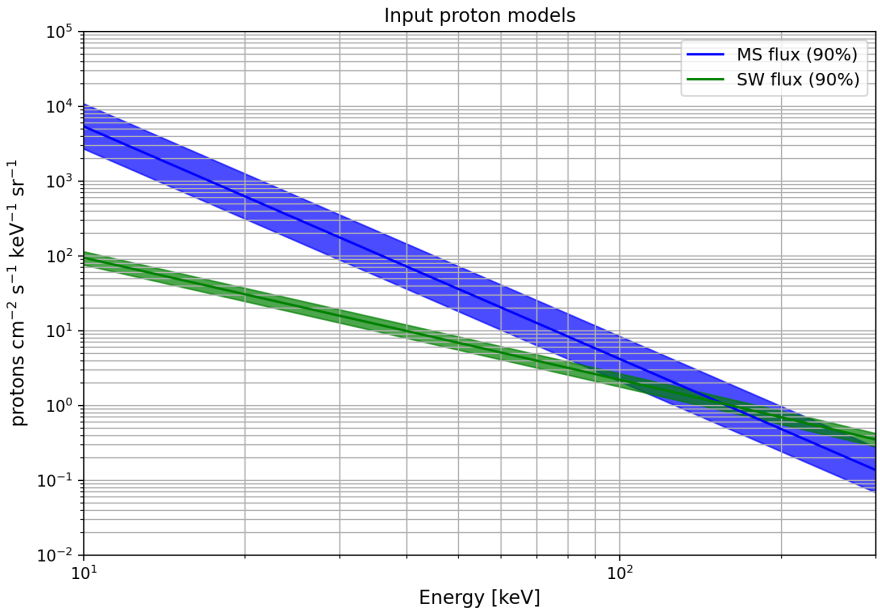

Figure 28: Proton spectral models used as input in the verification and validation activity.

In *Xspec*, the background flux, in cts cm^{-2} s^{-1} keV^{-1}, is obtained by convolving the input model with the RMF and ARF files. We note that since the ARF stores the grasp of the telescope, the input model is in *steradiant* units. The standard simulation is done by computing the simulated exposure to the input flux and dividing by the energy bins. Both spectra are normalised for the detector area. The result is shown in

Fig. 29 - 32 for the MS (left) and the SW (right) input models. The same background spectra are predicted from the standard simulation method and the use of the proton response files produced by this work.

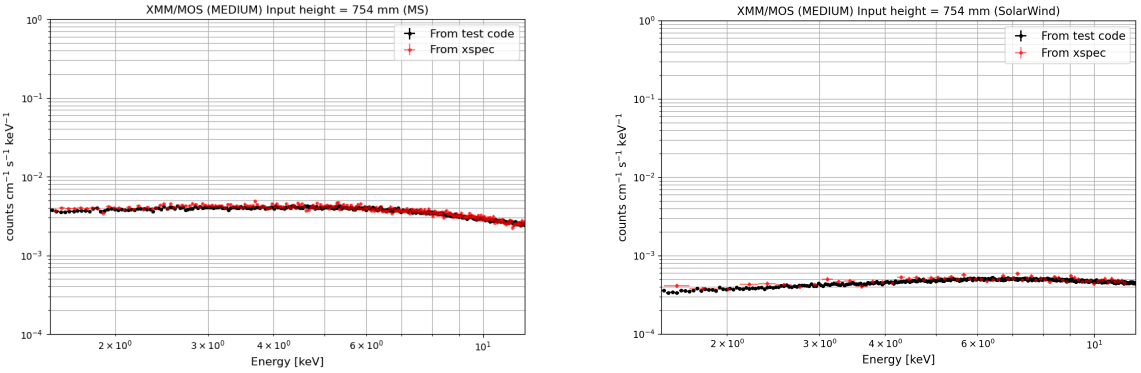

Figure 29: Comparison between a MOS standard simulation, using a power-law in input and obtained with *Xspec* using the proton response files, for an MS (left) and SW (right) input model.

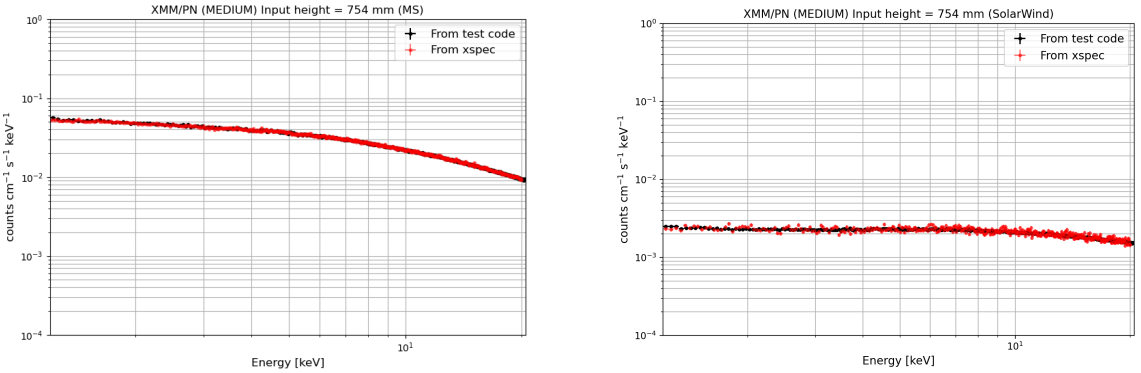

Figure 30: Comparison between a PN standard simulation, using a power-law in input, and obtained with *Xspec* using the proton response files, for an MS (left) and SW (right) input model.

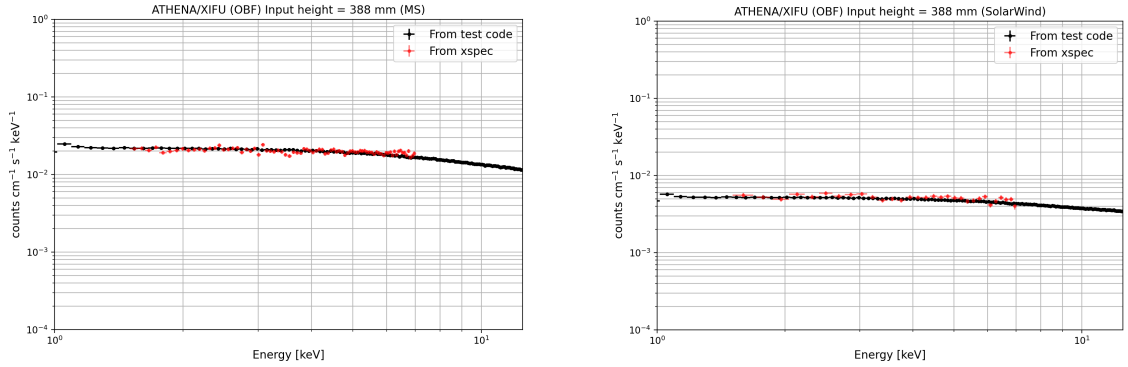

Figure 31: Comparison between an X-IFU standard simulation, using a power-law in input, and obtained with *Xspec* using the proton response files, for an MS (left) and SW (right) input model.

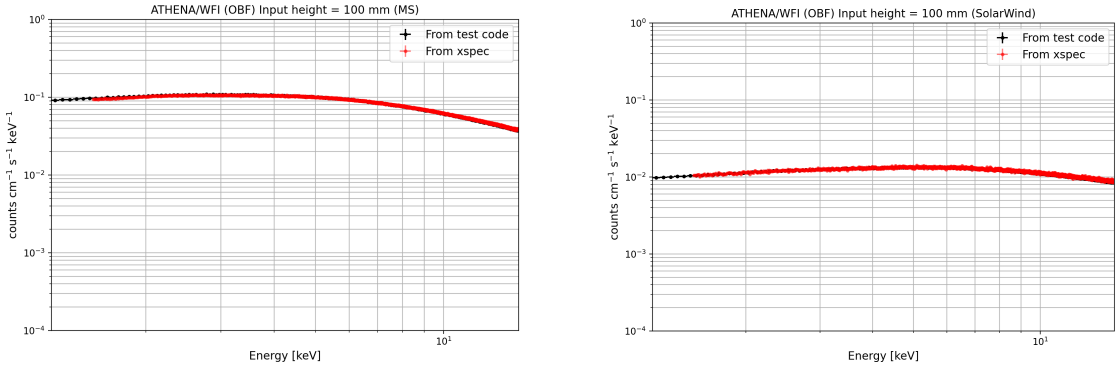

Figure 32: Comparison between a WFI standard simulation, using a power-law in input, and obtained with *Xspec* using the proton response files, for an MS (left) and SW (right) input model.

3.4 Validation of the XMM-Newton proton response files (Task 3.4)

The proton response matrices produced with the telescope end-to-end simulation need to be validated using real data. To this purpose, two kinds of analysis have been performed: the first considers data from single observations where both PN and MOS were available, and the second uses a representative MOS spectrum for the maximum rate expected in 90% of observation time, obtained from 12 years of observations (see Sect. 1.1).

3.4.1 Validation with single observations

Data from each considered set are reduced following the standard procedure using the XMM-Newton Science Analysis System (SAS v. 19.0.1). The MOS and PN data were processed with *emproc* and *epproc* tasks respectively and “Single” (PATTERN=0) pixel event patterns were selected for both detectors to be compliant with the proton response matrices.
Soft proton (SP) counts were extracted without any spatial selection using light curves in time bins of 100 s to identify the period where high background levels contaminated the scientific observation. Intervals

with rate > 10 c/s for PN and > 3 c/s for MOS were considered for the flare spectra accumulation. The background spectra were accumulated, identifying the time interval suitable for scientific observations of X-ray sources in the field of view. In particular, the intervals considered are those where the PN rate was < 4 c/s and where the MOS rate was < 2 c/s for ID 0000110101 and < 1 c/s for ID 0049150301 and ID 0864330201. Fig. 29 shows the flare (blue rectangle) and background intervals (red rectangle) selected for the analysis of ID 0049150301.
Information on the observations considered for this analysis is shown in Table 3. The energy range considered for the analysis is 2.0-11.5 keV.

	ID 0000110101		**ID 00049150301**		**ID 0864330201**	
Obs. Date	2001-08-19		2002-06-16		2020-01-10	
Duration (s)	15505		8250		141000	
Filter	MEDIUM		THIN1		THIN1	
	PN (c/s)	MOS(c/s)	PN (c/s)	MOS(c/s)	PN (c/s)	MOS (c/s)
SP Rate*	34.7	8.17	62.9	15.5	69.45	8.66
Bkg rate*	1.70	0.58	1.32	0.37	2.43	0.61

*The rate is computed in the energy range 2.0-11.5 keV.

Table 3: Log of the observations used for the analysis

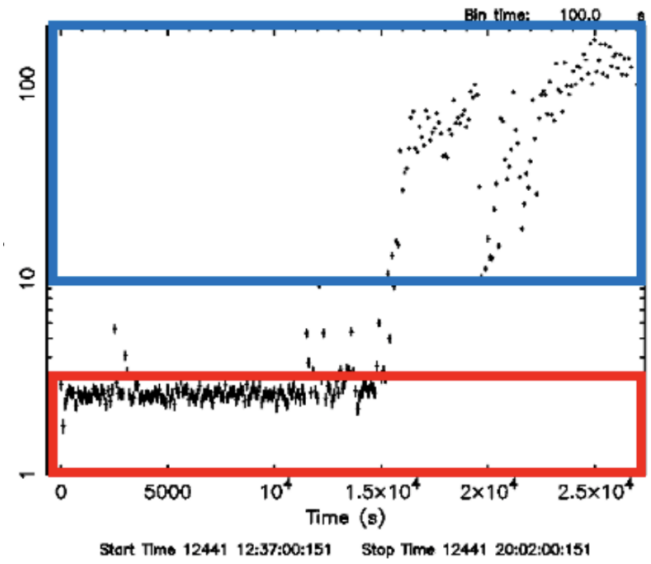

Figure 29: Light curve relative to PN observation of ID 0049150301 binned in 100 seconds. The blue and red rectangles identify the time interval used to collect soft protons and the background spectra, respectively.

From the spectral analysis, the following points have been derived:

- A single power law is not able to fit the entire energy range 2.0-11.5 keV either for MOS or PN in none of the observations. Fig. 30 shows, as an example, the fitting relative to the PN spectrum of ID 0000110101.
- A single power law is able to fit the range 5-11.5 keV in both observations with a spectral index 20±1% higher in the MOS with respect to the PN. The discrepancy between MOS and PN increases to 60% in the lower range 2-5 keV with the MOS steeper than the PN.

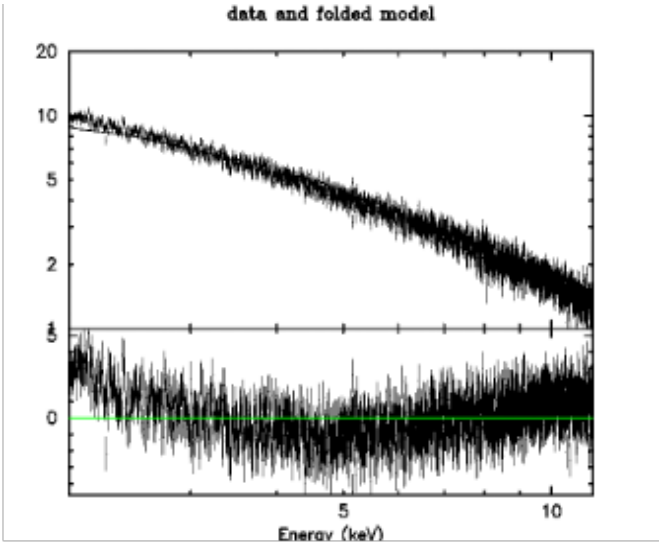

Figure 30: Fit with a single power-law of the ID 0000110101 PN spectrum.

	00049150301			**0000110101**			**ID 0864330201**		
	PN	MOS	MOS/ PN	PN	MOS	MOS/ PN	PN	MOS	MOS/ PN
KT (keV)	1.9±0.1	=PN		1.6±0.1	=PN		1.85±0.04	=PN	
Norm bbody	$(4.0^{+5.5/-6.3})\ 10^4$	$(1.7^{+0.8/-0.4})10^6$	**42**	$(7.4^{+1.3/-2.2})10^4$	$(4.5^{+3.7/-1.8})10^6$	**61**	<2.1e2	$(1.5^{+0.3/-0.3})10^6$	**>7e3**
α	3.4±0.1	=PN		3.8±0.1	=PN		3.78±0.01	=PN	
Norm pow	$(5.2^{+3.0/2.1})10^7$	$(1.2^{+0.8/-0.5})10^8$	**2.3**	$(1.1±0.4)10^8$	$(3.5±1.2)10^8$	**3.2**	$(2.3^{+0.5/-0.5})10^8$	$(2.5^{+0.7/-0.8})10^8$	**1.08**
χ^2 (dof)	1.03(1699)	1.00(566)		1.07(1699)	1.12(566)		1.21(1699)	1.01(566)	

Table 4: Spectral analysis results. The fitting model is a blackbody plus a power law.

Fitting MOS and PN with the common model composed of a low energy blackbody and a power law in the range 3-11.5 keV and fixing the spectral index and the temperature to the same value in both spectra gives, we obtain the best-fit parameters listed in Table 4. A blackbody + powerlaw model is a good interpretation of the observed spectra of MOS and PN. While the normalisation of the power-law varies with a factor ranging from 1 to 3 which can be considered consistent with the general uncertainties of the proton response files, the blackbody normalization changes considerably in the two instruments and in different observations of the same instrument. As shown in Table 4, the ratio of the MOS and PN blackbody normalization factors is about 40-60 in the first two observations, while in the third we only find an upper limit for the PN soft excess.

3.4.2 Validation with orbit averaged spectra

The soft proton spectrum detected by the EPIC MOS with the medium filter and extracted from almost 200 ks of observations at a high contamination state, reported in Sect. 1.1, was fitted with a black-body + powerlaw model using the proton response files for MOS medium filter configuration. The presence of a soft excess is also found in the averaged spectrum and we are also able to find a sufficient best-fit (red. χ^2 = 1409/566) only by cutting the spectrum at 3 keV (Fig. 31, left). The best-fit parameters are listed in Table 5. The fit is not optimal because of an additional soft excess that the black-body cannot explain and a bump at 5 keV. Since a dedicated spectral analysis of soft proton flares is outside the scope of this work, we find the best fit model to sufficiently describe - given the general uncertainties of the response files - the observed spectrum.
The best fit model, normalized for the maximum rate observed in 90% of the exposure, is compared with the Solar Wind and the Magnetosheath spectra. The latter are obtained for the maximum flux observed in 90% of operational time of in-flight radiation monitoring data. The result is shown in Fig. 31 (right), with a 50% uncertainty applied to the best-fit model. Both the intensity and slope of the power-law component are in good agreement with the MS model.

Parameter	Value
kT (bbody)	1.75 +/- 0.02
norm (bbody)	(2.5 +/- 0.3) $\times 10^7$
photon index (pow)	3.52 +/- 0.02
norm (pow)	(7.2 +/- 0.1) $\times 10^7$

Table 5: Best fit parameters from the analysis of the MOS spectrum.

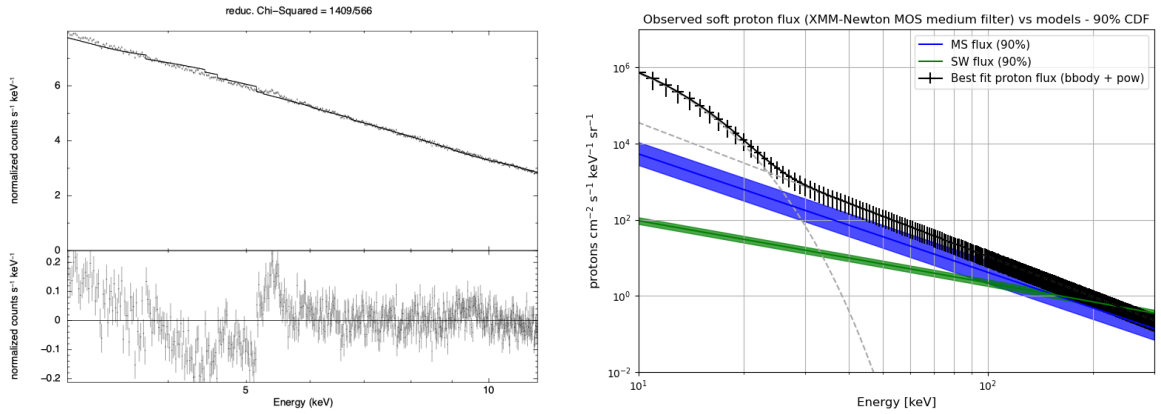

Figure 31: (left) Best fit model of the MOS (medium filter) averaged spectrum obtained from high contamination states. (right) Comparison between the MS and SW input proton models and the best-fit model normalized for the maximum rate observed at 90% of the exposure.

3.4.3 Summary of the validation activity

An actual validation of the proton response files would require generating at the SPO entrance low energy proton beams and measuring on-ground the effect of their transmission through the mirror and the FPA filters. Since this is not - yet - possible, we validated our simulation with in-flight data while in principle not knowing the proton population entering the mirror.
We can state that in general the response files can successfully analyse or simulate the spectra above an observed 5-6 keV lower limit both in terms of the predicted flux and the spectral distribution at the focal plane. Below these energies, we found a soft excess varying between simultaneous MOS and PN observations and with respect to the power-law component. Further studies are required to assess the origin of the soft excess. While it is not the scope of this validation activity to study the origin of XMM-Newton soft proton flares, we could speculate that there is a power-law component that arises above 30-40 keV than is consistent with the proton fluxes measured in the magnetotail. At low energies, we found instead an excess that because of its varying nature could be either linked to additional background components or limitations in the accuracy of the proton response files.

References

[1] Turner, M. J. L. et al., “The European Photon Imaging Camera on XMM-Newton: The MOS cameras,” A&A 365, L27–L35 (2001).

[2] Struder, L. et al., “The european photon imaging camera on xmm-newton: The pn-ccd camera,” A&A 365, L18–L26 (2001).

[3] den Herder, J. W. et al., “Performance of the reflection grating spectrometer CCD detectors onboard XMM-Newton,” Proc. SPIE 5501, 32–43 (2004).

[4] Nartallo, R. et al., “Radiation Environment Induced Degradation on Chandra and Implications for XMM-Newton,” Esa/estec/tos-em/00-015/RN Tech. Report (2002).

[5] Jansen, F. et al., “Xmm-newton observatory. i. the spacecraft and operations,” A&A 365, L1–L6 (2001).

[6] Marelli, M. et al., “A systematic analysis of the XMM-Newton background: I. Dataset and extraction procedures,” Experimental Astronomy 44(3), 297–308 (2017).

[7] Molendi, S. et al., “Radiation Background Data Analysis & Lessons Learned from Previous X-ray Missions”, AREMBES WP1 TN 1., 2017

[8] Agostinelli, S. et al., “Geant4–a simulation toolkit,” NIM A 506, 250 – 303 (2003).

[9] Allison, J. et al., “Geant4 developments and applications,” IEEE Trans. Nucl. Sci. 53(1), 270 –278 (2006).

[10] Fioretti, V. et al., “The Geant4 mass model of the ATHENA Silicon Pore Optics and its effect on soft proton scattering”, Proc. SPIE, 106993J (2018)

[11] Diebold, S. et al., “Updates on experimental grazing angle soft proton scattering,” Proc. of SPIE 10397, 103970W (2017).

[12] Fioretti, V. et al., “Geant4 simulations of soft proton scattering in X-ray optics. A tentative validation using laboratory measurements,” Experimental Astronomy 44(3), 413–435 (2017).

[13] Molendi, S. et al., “EXACRAD final report”, ESA Tender (2021)

[14] Fioretti, V. et al., “EXACRAD WP 8.1 final report”, EXACRAD TN (2021)

[15] Henke, B. L., Gullikson, E. M., and Davis, J. C., “X-Ray Interactions: Photoabsorption, Scattering, Transmission, and Reflection at E = 50-30,000 eV, Z = 1-92,” Atomic Data and Nuclear Data Tables 54(2), 181–342 (1993).

[16] Owens, A. et al., “Measuring reflected x-ray absorption fine structure in gold-coated x-ray mirrors,” Proc. of SPIE 2279, 325–331 (1994).

[17] Remizovich, V. S., Ryazanov, M. I., and Tilinin, I. S., “Energy and angular distributions of particles reflected in glancing incidence of a beam of ions on the surface of a material,” Sov. J. Exp. Th. Phys. 52, 225 (1980).

[18] Amato, R. et al., “Soft proton scattering at grazing incidence from X-ray mirrors: analysis of experimental data in the framework of the non-elastic approximation,” Experimental Astronomy 49(3), 115–140 (2020).

[19] Mineo, T. et al., “An XMM-Newton proton response matrix”, Exp. Astr., 44, 3 (2017)

[20] Holland, A. D. et al., “MOS CCDs for the EPIC on XMM,” Proc. of SPIE 2808, 414–420 (1996).

[21] Hiraga, J. et al., “Direct measurement of sub-pixel structure of the EPIC MOS CCD on-board the XMM//NEWTON satellite,” NIM A 465(2-3), 384–393 (2001).

[22] Fraser, G. W. et al., “Potential solar axion signatures in X-ray observations with the XMM-Newton observatory,” MNRAS 445(2), 2146–2168 (2014).

[23] Nandra, K., et al., “The Hot and Energetic Universe: A White Paper presenting the science theme motivating the Athena+ mission”, White Paper (2013)

[24] Meidinger, N. et al., “The Wide Field Imager instrument for Athena,” Proc. of SPIE 10397, 103970V (2017)

[25] Barret, D. et al., “The Athena X-ray Integral Field Unit: a consolidated design for the system requirement review of the preliminary definition phase, Proc. SPIE", 121810L (2022)

[26] Lotti, S. et al., “Soft proton flux on ATHENA focal plane and its impact on the magnetic diverter design”, Exp. Astr. 45, 411–428 (2018)

[27] Fioretti, V. et al. “Magnetic Shielding of Soft Protons in Future X-Ray Telescopes: The Case of the ATHENA Wide Field Imager”, ApJ, 867, 9 (2018)

[28] Athena Study team, “ATHENA - Telescope Reference Design and Effective Area Estimates”, ESA-ATHENA-ESTEC-PL-DD-0001, v3.3, 21/12/2020

[29] Lotti, S. et al., “Review of the Particle Background of the Athena X-IFU Instrument”, ApJ, 909, 111 (2021)

Deliverables

The proton RMF and ARF files are available for download without restriction at the following INAF gitlab repository:

https://www.ict.inaf.it/gitlab/proton_response_matrix

Dissemination & communication activities

Conferences:

- SPIE OP314 (Optics for EUV, X-Ray, and Gamma-Ray Astronomy X) 2021 poster and conference proceeding with the title “Design and characterization of a prototype proton response matrix for the XMM-Newton mission”

Deviations and non-compliances

There are no deviations or non-compliances at the moment. There are however some limitations when using the current release of the proton response files:

- a total uncertainty of 50% must be assigned to any result produced with the response files since many approximations or assumptions were required along the work;
- the MOS is covered by a non-uniform electrode structure that strongly affects the energy redistribution of the protons. While the 60% to 40% surface coverage of the two different electrodes was verified with the measured X-ray transmission, the continuous energy losses in the proton interaction while crossing the read-out device could produce unwanted effects that the Geant4 itself cannot reproduce. Also, small discrepancies in the X-ray transmission could translate into larger differences when considering the proton stopping power.
- The limited statistics of the simulations were underestimated in writing the proposal hence no funding was dedicated to the purchase of run time in external computing services. This led to randomly sampling the proton distribution and using interpolation functions for the energy redistribution, which limited the validity energy ranges of the response files.